HHS Public Access

Author manuscript

Neuron. Author manuscript; available in PMC 2021 May 20.

Published in final edited form as:

Neuron. 2020 May 20; 106(4): 624–636.e4. doi:10.1016/j.neuron.2020.02.029.

Periaqueductal gray and rostromedial tegmental inhibitory afferents to ventral tegmental area have distinct synaptic plasticity and opiate sensitivity

St. Robyn Laurent[1,3], **Valentina Martinez Damonte**[1], **Ayumi C. Tsuda**[2], **Julie A. Kauer**[1,4,*]

[1]Department of Psychiatry and Behavioral Sciences, Stanford University School of Medicine, Stanford, CA 94035, USA

[2]Department of Molecular Pharmacology, Physiology, and Biotechnology, Brown University, Providence, RI 02912, USA

[3]Present address: Gladstone Institutes, 1650 Owens Street, San Francisco, CA 94158, USA

[4]Lead Contact

Summary

The ventral tegmental area (VTA) is a major target of addictive drugs, and receives multiple GABAergic projections originating outside the VTA. We describe differences in synaptic plasticity and behavior with optogenetically driving two opiate-sensitive GABAergic inputs to the VTA, the rostromedial tegmental nucleus (RMTg) and the periaqueductal gray (PAG). Activation of GABAergic RMTg terminals in the VTA *in vivo* was aversive, and low frequency stimulation induced long term depression *in vitro.* Low frequency stimulation of PAG afferents *in vitro* unexpectedly caused long term potentiation. Opioid receptor activation profoundly depressed PAG and RMTg inhibitory synapses but prevented synaptic plasticity only at PAG synapses. Activation of the GABAergic PAG terminals in the VTA promoted immobility, and optogenetically-driven immobility was blocked by morphine. Our data reveal the PAG as a source of highly opioid-sensitive GABAergic afferents and support the idea that different GABAergic pathways to the VTA control distinct behaviors.

eTOC

The ventral tegmental area contains many subcircuits that control a diverse repertoire of behavior. St. Laurent et al. find that two different presynaptic sources of inhibition that show opposite

[*]**Correspondence:** jkauer@stanford.edu.

Author Contributions

RS designed, performed, and analyzed physiology and behavioral experiments. VMD performed and analyzed physiology experiments. RS and AT performed all immunohistochemistry and imaging. RS, VMD, and JK designed, discussed and analyzed data. RS, VMD, AT, and JK contributed to the preparation of the manuscript and figures.

Declaration of Interests

The authors declare no competing interests.

synaptic plasticity features after the same stimulus pattern that are differentially regulated by opioids and mediate distinct behaviors.

Graphical Abstract

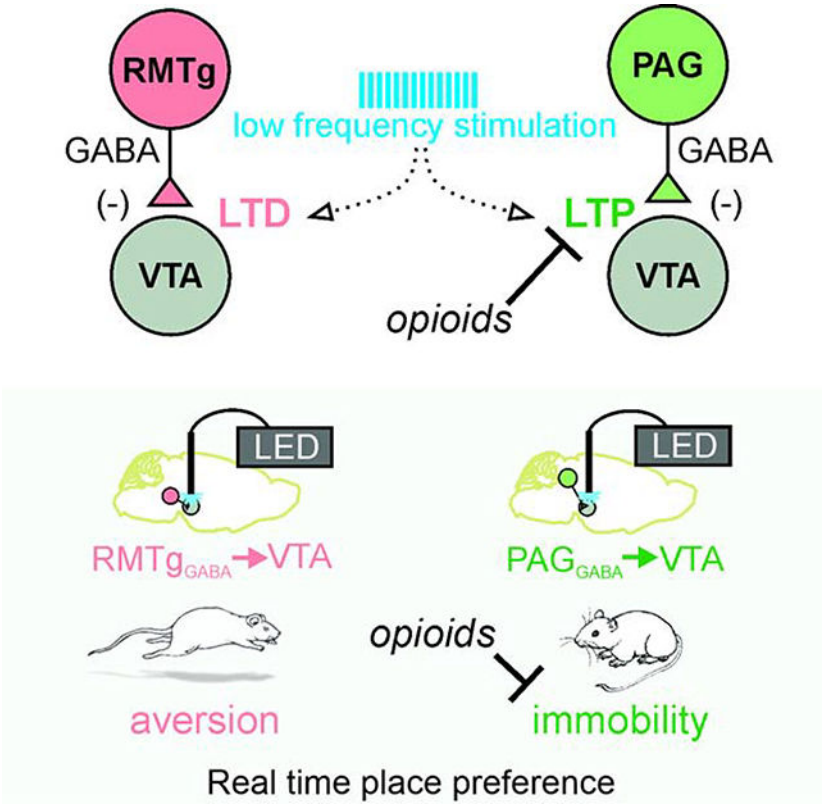

Keywords

dopamine; GABA; plasticity; morphine; electrophysiology; behavior; aversion; PAG; RMTg; opiates

Introduction

The ventral tegmental area (VTA) encodes information about both rewarding and aversive stimuli, and is required for the addictive properties of drugs of abuse (Nestler, 2004, Jones and Bonci, 2005, Mazei-Robison and Nestler, 2012). The VTA receives inhibitory input from local interneurons, but also from numerous extrinsic brain areas (Beier et al., 2015). Opiate drugs inhibit GABAergic cells that normally regulate dopamine cell firing, increasing their firing rate (Johnson and North, 1992, Gysling and Wang, 1983, Steffensen et al., 2006, Ford et al., 2006, Matsui and Williams, 2011). Deciphering the effect of opioids in the VTA is a complex task, however, as the relative suppression by opioids differs among GABAergic sources (Matsui et al., 2014). This is further complicated by the divergent roles that VTA dopamine cells themselves have in regulating reward or aversion (Lammel et al., 2011). To place the relative contribution of opioid effects into context, it is essential to understand the

heterogeneous properties of different VTA afferents using genetic and anatomical isolation of afferent populations (Lammel et al., 2014, Pathan and Williams, 2012).

Here we characterize opiate sensitivity, synaptic plasticity, and behavioral output of two distinct GABAergic projections that inhibit VTA dopamine neurons. One major source of GABAergic inhibition to the VTA originates in a neighboring midbrain region, the rostromedial tegmental nucleus (RMTg) (Jhou et al., 2009b). The RMTg receives excitatory glutamatergic projections from the lateral habenula that are required for behavioral responses reflecting strong aversion, including passive, active and conditioned avoidance (Stamatakis and Stuber, 2012, Jhou et al., 2009a). The aversive nature of this stimulation results in part from inhibition by the RMTg cells of the VTA dopamine cells they innervate (Jhou et al., 2009a, Hong et al., 2011, Vento et al., 2017; Li et al., 2019), but we do not yet have a complete understanding of RMTg-driven behavior or plasticity, for example whether triggers exist that persistently downregulate this strong source of VTA dopamine inhibition. A defining feature of $RMTg_{GABA}$→VTA synapses is that they are more robustly depressed by μ-opioid receptor (μOR) activation than other sources of GABAergic inhibition in the VTA, including local VTA interneurons and nucleus accumbens projections (Matsui and Williams, 2011, Matsui et al., 2014), and strongly regulate VTA dopamine cell firing (Jalabert et al., 2011). Surprisingly however, these opioid-sensitive GABAergic synapses do not exhibit a form of synaptic plasticity known to be blocked after a single *in vivo* morphine exposure, LTP_{GABA} (Nugent et al., 2007, Simmons et al., 2017, Polter et al., 2018). It is not known whether $RMTg_{GABA}$→VTA synapses can express other forms of synaptic plasticity, such as long-term depression (LTD_{GABA}) also blocked by in vivo morphine (Dacher and Nugent, 2011, Dacher et al., 2013).

Another highly opioid-sensitive brain region is the periaqueductal gray (PAG). The PAG is required for diverse opiate actions, as morphine administration into the PAG produces analgesia (Jensen and Yaksh, 1989, Lewis and Gebhart, 1977, Mayer et al., 1971, Campion et al., 2016), opioid receptor antagonists in the PAG precipitate morphine withdrawal (Laschka and Herz, 1977), and microinjections targeting either the PAG or VTA induce conditioned place preference (Olmstead and Franklin, 1997). The PAG is organized into longitudinal columns that dictate connectivity and behavioral outputs to pain, stress, and threats: dorsal subdivisions (dPAG) are associated with the generation of both active and passive responses (including e.g. both freezing and flight) while ventral PAG subdivisions (vPAG) are generally associated only with coordination of passive behaviors (Bandler and Shipley, 1994, Bandler and Keay, 1996, Vander Weele et al., 2018, Wright and McDannald, 2019, Lefler et al., 2020), and analgesia is also most profound when morphine is locally targeted to the caudal portion of the ventrolateral region (Yaksh et al., 1976). The vPAG sends both glutamatergic and GABAergic projections to the VTA (Omelchenko and Sesack, 2010, Ntamati et al., 2018, Faget et al., 2016; Waung et al., 2019) that are non-catecholaminergic (Suckow et al., 2013). Activating the ventrolateral PAG induces quiescence, i.e. reduced spontaneous activity (Depaulis et al., 1994). A recent study reported that the GABAergic vPAG cells also enhances anxiety phenotypes and inhibits conditioned fear responses, without affecting freezing per se (Lowery-Gionta et al., 2018). Despite these intriguing findings, the functional relevance of $RMTg_{GABA}$→VTA synapses is poorly defined and has received far less attention than the $RMTg_{GABA}$→VTA pathway. Here, using

an optogenetic approach to compare the physiological, plastic, and behavioral properties of these two GABAergic afferent pathways to the VTA we found striking differences.

Results

$RMTg_{GABA}$→VTA synapses undergo long-term depression

Recent reports from our lab and others have demonstrated that plasticity of GABAergic synapses in the VTA is afferent-specific; both groups independently found that the RMTg afferents do not exhibit nitric oxide-dependent LTP (LTP_{GABA}) (Simmons et al., 2017, Polter et al., 2018). We asked whether RMTg synapses can exhibit another form of plasticity: low frequency stimulation-induced LTD (LFS-LTD_{GABA}), first reported using local electrical stimulation (Dacher and Nugent, 2011). We used an optogenetic strategy, injecting an adeno-associated virus into the RMTg of a VGAT-IRES-Cre mouse to express channelrhodopsin (AAV2-DIO-ChR2-mCherry). Several weeks later, we prepared acute midbrain slices and selectively drove RMTg afferents while recording in VTA cells (Figure 1A; Figure S1A–B). We optically evoked GABAergic IPSCs using brief LED pulses (oIPSCs) in VTA cells that had a hyperpolarization-induced current (I_h); in a subset of experiments, cells were additionally validated using a Pitx3:GFP line in which dopamine cells can be identified (Figure S1D) (Maxwell et al., 2005). After establishing a stable baseline of oIPSCs, delivery of optical low-frequency stimulation (oLFS: 1 Hz, 6 minutes during depolarization to −40 mV) modestly depressed RMTg GABAergic oIPSCs recorded in VTA cells (77 ± 8% of baseline, n = 13 cells; Figure 1B–E). Furthermore, this LTD persisted in the presence of the NMDAR antagonist, d-APV (Figure 1C–E). The baseline amplitude was not correlated with depression magnitude (Figure S1C). LFS-LTD_{GABA} was previously shown to be attenuated by dopamine D2 receptor antagonists (Dacher and Nugent, 2011), most likely as a result of somatodendritic dopamine release activating D2 receptors and opening GIRK channels (Beckstead et al., 2004). To minimize local dopamine release, we voltage-clamped the cells at −70 mV during oLFS, and found that RMTg oIPSC amplitude was no longer depressed after 6 minutes of 1 Hz stimulation (103 ± 14% of baseline, n = 7 cells; Figure S1E–G), suggesting that presynaptic stimulation alone is insufficient to induce this form of plasticity, and consistent with mechanisms underlying LTD_{GABA} (Dacher and Nugent 2011).

Synaptic alterations within circuits that govern opiate-related behavior could represent a mechanism for critical early changes in the reward pathway in the development of addiction. A single in vivo exposure to morphine alters known forms of synaptic plasticity in the VTA, including LTP at excitatory synapses (Saal et al., 2003) and LTP_{GABA} and LTD_{GABA} at inhibitory synapses (Nugent et al., 2007, Dacher and Nugent, 2011). RMTg cells are hyperpolarized by a pOR agonist [D-Ala2, N-MePhe4, Gly-ol]-enkephalin (DAMGO) (Matsui and Williams, 2011) and RMTg IPSCs in the VTA are depressed by μOR activation (Matsui et al., 2014). Opioids therefore can acutely increase VTA dopamine cell firing by hyperpolarizing RMTg GABAergic cells and reducing GABA release from their synapses on VTA dopamine cells (Johnson and North, 1992, Gysling and Wang, 1983, Steffensen et al., 2006, Ford et al., 2006, Matsui and Williams, 2011). As reported previously, DAMGO depressed oIPSC amplitude from RMTg afferents in VTA cells (40 ± 5% of baseline; Figure

1F–G). To test whether acute exposure to opiates also regulates the induction of LTD at $RMTg_{GABA}$→VTA synapses, we measured LTD induced in the presence of DAMGO, and found that LTD was unaffected (LTD: 75 ± 9% of baseline; Figure 1H–J). RMTg synapses undergo LTD with LFS paired with mild postsynaptic depolarization, independently of μOR activation.

Activating $RMTg_{GABA}$→VTA synapses is aversive

Silencing local GABAergic interneurons in the VTA induces appetitive behaviors (Jennings et al., 2013), while activation of these interneurons is aversive and disrupts reward consumption (Tan et al., 2012, Van Zessen et al., 2012). Similarly, optogenetic activation of lateral habenula excitatory inputs on RMTg cells at 60 Hz in vivo results in robust place aversion (Stamatakis and Stuber, 2012). We therefore measured place aversion to stimulation of $RMTg_{GABA}$ terminals in the VTA using a real-time place preference procedure (RTPP; Figure 2A). We injected AAV-DIO-ChR2-mCherry in the RMTg of VGAT-IRES-Cre mice and implanted a light fiber above the VTA (Figure 2B, S2A–B). The RMTg typically has a high spontaneous firing rate, reportedly 3–9 Hz in vitro and 10–30 Hz in vivo (Lecca et al., 2011, Jalabert et al., 2011) but the firing rate can increase to 50 Hz or more during presentation of aversive stimuli, such as a strong footshock or mechanical stimulation (Lecca et al., 2011). We used 60 Hz optical stimulation in the VTA to drive RMTg synapses at a frequency that produced robust IPSCs in VTA neurons in vitro (Figure S2E–F). ChR2-expressing mice reduced the time spent in the light-paired chamber compared with mice expressing the reporter only ($F(1, 10) = 10.66$, $p = 0.009$; 60 Hz light test: reporter only 38 ± 13 s, ChR2 −67 ± 22 s; n = 6 mice/group; $p = 0.02$; Figure 2B, 2E, see supplemental video example). Avoidance persisted in a posttest conducted 24 hours later without light stimulation (reporter only 6 ± 27 s, ChR2 −95 ± 37 s, n = 6 mice; $p = 0.02$; Figure 2B). During the light tests and post-tests, ChR2 mice decreased the number entries into the light chamber compared to pretest values (Figure S2C), while the mean velocity in the light vs. pretest and total distance traveled vs. pretest were not significantly different (velocity: $F (1, 10) = 1.89$, $p = 0.20$, distance: $F (1, 10) = 0.64$, $p = 0.44$; Figure 2C–D). Furthermore, gross locomotor activity was unaffected by light stimulation as performance on a rotarod test with and without 60 Hz light stimulation did not differ between ChR2 and reporter only mice (Figure S2D). These data support our hypothesis that activation of GABAergic RMTg synapses in the VTA is aversive. As in all such studies, our in vivo optical stimulation must be interpreted conservatively, given the possibility of activation of axon collaterals to other brain regions or fibers of passage. RMTg projections are strongest to the VTA and substantia nigra, so a light fiber placed above the VTA could in theory provide some activation of axons to the neighboring substantia nigra. However, our observation of aversion is consistent with previous observations of aversion during local inhibition of VTA dopamine neurons (Tan et al., 2012, Van Zessen et al., 2012) and less so with inhibition of SNc neurons (Saunders et al., 2018).

$vPAG_{GABA}$→VTA synapses display an unusual form of LTP after low frequency stimulation

In contrast to afferents originating in the RMTg, plasticity and behavior at GABAergic afferents from $vPAG_{GABA}$→VTA has never been investigated. We first targeted ChR2 to the PAG using AAV-hsyn-ChR2-EYFP (Figure 3A, S3A), and pharmacologically isolated

GABAergic synaptic currents in VTA cells in slices from these animals by blocking glycine and AMPARs during afferent light pulse stimulation (Figure S3B). We then tested the same oLFS protocol that induced LTD in RMTg→VTA synapses. Surprisingly, rather than triggering LTD, oLFS of vPAG GABAergic oIPSCs instead triggered robust LTP (149 ± 15% of baseline amplitude, n = 15 cells; Figure 3B–D, S3C–D). Potentiation was induced in the presence of d-APV, indicating that NMDAR activation was not required for LTP induction. To drive GABAergic PAG_{GABA}→VTA synapses selectively, we repeated these experiments using viral injections of AAV-DIO-ChR2-mCherry in VGAT-cre mice to infect only VGAT-expressing cells (Figure 3E, S3A). Using this optogenetic strategy, oLFS still elicited LTP of PAG oIPSCs (129 ± 11 % of baseline amplitude, n = 9 cells; Figure 3F–H).

We carried out several experiments to clarify the mechanisms underlying oLFS-induced LTP. We thought that oLFS might release a neurotransmitter or peptide in addition to GABA that acts on a postsynaptically located GPCR required for LTP induction (Lante et al., 2006, Gibson et al., 2008, Gonzalez et al., 2014). To test this possibility, we included GDP-βS (1 mM) in the recording pipette to prevent GPCR signaling in the postsynaptic cell. However, oLFS of PAG afferents elicited robust LTP under these conditions (147 ± 16% of baseline amplitude, n = 5 cells, Figure S4A–C). Similar to LFS-LTD_{GABA} elicited at RMTg synapses, mild depolarization was required for LTP induction, because when the cell was voltage-clamped at −70 mV during the oLFS protocol, oLFS failed to induce LTP (96 ± 9% of baseline amplitude, n = 6 cells; Figure S4D–F). Postsynaptic intracellular Ca^{2+} is required for many forms of plasticity, including NMDAR-independent forms (Gibson et al., 2008, Heifets and Castillo, 2009, Luscher and Huber, 2010), and we therefore next included BAPTA (30 mM) in the recording pipette, to chelate postsynaptic intracellular Ca^{2+}. This manipulation also prevented LTP, indicating that a rise in postsynaptic calcium during oLFS is required for LTP induction (95 ± 8% of baseline amplitude, n = 7 cells, Figure S4G–I). Together our results favor a mechanism that does not require postsynaptic GPCRs but may depend on non-NMDAR mechanisms of postsynaptic depolarization and Ca^{2+} influx.

Opioid-receptor activation blocks LTP of PAG_{GABA}→VTA synapses

Like RMTg neurons, GABAergic cell bodies in the PAG are robustly hyperpolarized by μOR activation (Vaughan et al., 2003), however, the effect of opioids on vPAG synapses in the VTA is not known. DAMGO potently but reversibly depressed vPAG olPSCs (24 ± 6% of baseline amplitude, n = 10 cells; Figure 3I–J). PAG olPSCs were depressed even more than RMTg olPSCs at this concentration of DAMGO (Figure S4J). Moreover, 1 μM DAMGO in the bath also entirely prevented LTP induction by oLFS at PAG synapses (olPSC amplitude after oLFS: 76 ± 9% of baseline, n = 7 cells, Figure 3K–M). Thus, GABAergic PAG synapses on VTA neurons are robustly depressed and are no longer capable of exhibiting LTP in the presence of opioids.

Activating $vPAG_{GABA}$→VTA synapses *in vivo* increases immobility

Despite a wealth of literature detailing PAG-mediated behaviors, the outcome of specifically activating $vPAG_{GABA}$→VTA synapses in vivo is unknown. Activating the vPAG induces quiescence or freezing (Depaulis et al., 1994, Keay and Bandler, 2001, Morgan and Carrive, 2001; Taylor et al., 2019b) while activating GABAergic cells in the vPAG facilitates

nociception (Samineni et al., 2017); the $vPAG_{GABA}$→VTA projection may participate in some of these behaviors. Given the role of the VTA in reward and aversion, we tested RTPP while activating this pathway; this simple behavioral test provides information not only on preference or aversion, but also on locomotor behavior and freezing. The experimental design also allowed us to perform within-group testing of in vivo low frequency stimulation just prior to the RTPP.

We expressed AAV-DIO-ChR2-mCherry in the vPAG of VGAT-cre mice, and first recorded in vitro from $ChR2^+$ cells within the vPAG during light trains. We found a robust light-induced increase in cell firing (Figure S5A); $VGAT^+$ cells within the PAG slices fired spontaneously in vitro (8.1 ± 1.1 Hz, n = 3 cells, data not shown), a range similar to that reported in vivo (Tovote et al., 2016). For behavioral assays, we chose a 20 Hz frequency, which is higher than this basal firing rate and had high spike fidelity in the PAG (Figure S5A). We recorded from VTA cells in midbrain slices to assess the effect of light trains on VTA firing rate. Ramps of current induced action potential firing in VTA cells, while the same ramp with a concurrent 20 Hz train of LED pulses reduced firing in the same cell (Figure S5B); no persistent depression of firing was noted when the light was turned off. In the VTA, vPAG oIPSCs were triggered by optical stimulation at 20 Hz, and were blocked by bicuculline (Figure S5C).

For behavioral experiments, we targeted $vPAG_{GABA}$ cells selectively with a unilateral viral injection in the vPAG of VGAT-cre mice of either stop-floxed ChR2 (AAV-DIO-ChR2-mCherry) or a fluorescent reporter alone (AAV-DIO-EYFP or AAV-DIO-mCherry) and implanted a light fiber ipsilaterally in the VTA (Figure 4A and S5D–E). Projections of the PAG to brainstem nuclei do not apparently collateralize (Beitz et al., 1983), although PAG cells innervating the forebrain may branch to the nucleus raphe magnus and thalamus (Barbaresi et al., 1982; Li et al., 1990, Reichling and Basbaum, 1991), raising the possibility of optical activation of a subset of afferents to other brain regions, but only if these collaterals pass through the VTA where the light fiber would activate them. Testing consisted of a four-day RTPP procedure (Figure 4B): 1) a pretest without light stimulation, 2–3) two testing days consisting of 20 Hz light stimulation on one side of the apparatus, and 4) a posttest without light stimulation. On one of the light test days, mice received *in vivo* oLFS stimulation (1 Hz) for 6min in an empty 30 cm × 30 cm home cage, 15 min prior to the 20 Hz light test. Surprisingly, driving this GABAergic pathway to the VTA elicited a distinct behavioral profile compared with driving RMTg afferents. On light test days, mice in the opsin group exhibited a phenotype of intermittent halting in the light chamber when receiving photostimulation (see supplemental video, Figure 4C). We therefore measured time spent immobile (see Methods) and this analysis revealed an increased percentage of time immobile in the light-paired chamber compared to pretest values between experimental groups (Figure 4D; $F(1,15) = 9.72$, $p = 0.007$). Immobility in the light-paired chamber was significantly different between reporter-only and opsin groups in the light test without prior oLFS (reporter only −1 ± 5%, n = 7 mice, opsin 17 ± 5%, n = 10 mice) and with oLFS (reporter only 0 ± 5%, n = 7 mice, opsin 19 ± 4%, n = 10 mice). Although 1 Hz oLFS did not affect mean values for immobility (Figure 4D), the counterbalanced test order could mask such an effect. We separated the ChR2 group data by test order to determine if oLFS pretreatment augmented the effect of 20 Hz light stimulation. This analysis showed that

mice receiving LFS prior to the first 20 Hz light test exhibited more immobility than mice that first received 20 Hz light alone (Figure S5F; $F(3, 16) = 3.80$, $p = 0.031$), suggesting the possibility that LFS preconditioning enhanced the immobility phenotype.

Consistent with the immobile phenotype, the distance traveled in the apparatus vs. the pretest values also differed between experimental groups for both light test days (Figure 4E; $F(1,15) = 11.72$, $p = 0.004$; 20 Hz alone [reporter only 0.0 ± 0.3 m, opsin −1.2 ± 0.2 m], LFS/20 Hz light test [reporter only - 0.3 ± 0.2 m, opsin −1.1 ± 0.1 m]). Similarly, the mean velocity in the light-paired chamber vs. the pretest values also differed significantly between experimental groups for both light tests (Figure 4F; $F(1,15) = 8.01$, $p = 0.013$; 20 Hz light test alone [reporter only −0.4 ± 0.5 cm/s, opsin −2.0 ± 0.4 cm/s], LFS/20 Hz light test [reporter only −0.4 ± 0.6 cm/s, opsin −1.9 ± 0.2 cm/s]). Activity was slightly reduced across test days, most likely explained by habituation to the testing apparatus. We also performed a rotarod procedure with PAG terminal stimulation in the VTA. Light-induced immobility is unlikely to be explained by motor suppression as there were no deficits in motor performance on the rotarod (Figure S5G). Quantifying the overall time spent in the light-paired chamber compared to pretest values revealed no differences between groups during any test day (Figure 4G; $F(1,15) = 0.47$, $p = 0.50$). A posttest at 24 hours after the second light test also did not reveal conditioned place preference or aversion (Figure S5H).

Morphine blocks the vPAG$_{GABA}$→VTA immobility phenotype

As noted above, we found that opioids potently reduce GABAergic inhibition from PAG synapses in the VTA (Figure 3I–J; Figure S4K). Therefore, we hypothesized that *in vivo* morphine would essentially take this vPAG$_{GABA}$→VTA circuit offline, rendering optogenetic stimulation of PAG$_{GABA}$→VTA synapses ineffective at inducing the immobile phenotype. A separate cohort of mice consisting of three groups was used to compare the effect of light stimulation (Figure 5A) in the presence of morphine: 1) experimental: ChR2 mice receiving morphine, 2) negative control: reporter only mice receiving morphine, and 3) positive control: ChR2 mice receiving saline (Figure S5I–J). All mice were identically handled and habituated to intraperitoneal injections for two days prior to testing; all groups received a saline injection before the pretest, and on test day were given morphine (3 mg/kg i.p.) or saline 30 minutes prior to the RTPP procedure (Figure 5B), when all groups received light stimulation upon entering the light-paired chamber.

We found a significant difference between groups for percentage of time immobile in the light-paired chamber compared to pretest values ($F(2,18) = 8.5$, $p = 0.003$; Figure 5C). Consistent with our hypothesis, only the opsin + saline group increased their percentage of time spent immobile, while both morphine groups did not increase their immobility with light stimulation (opsin + SAL: 19 ± 2%, n = 7 mice; opsin + MOR: 7 ± 3%, n = 6 mice; reporter only + MOR: 2 ± 3%, n = 8 mice). The distance traveled in the apparatus vs. pretest values differed between experimental groups ($F(2,18) = 6.5$, $p = 0.007$; Figure 5D), again with the opsin + saline group traveling significantly less compared to both morphine groups (reporter only + MOR: −0.3 ± 0.2 m; opsin + MOR: −0.4 ± 0.2 m; opsin + SAL: −1.0 ± 0.2 m). These results could not be attributed to an overall difference in locomotion for the morphine group, as their change in distance traveled vs. the pretest was not significantly

different from the drug- free control group (Figure S5K). Mean velocity in the light-paired chamber vs. pretest values also differed among groups ($F(2,18) = 9.8$, $p = 0.001$; Figure 5E); with the opsin + saline group having reduced mean velocity compared to the two morphine groups (reporter only + MOR: 0.1 ± 0.3 cm/s; opsin + MOR: −0.6 ± 0.3 cm/s; opsin + SAL: −1.7 ± 0.3 cm/s). As with the drug-free RTPP test (Figure 4), there was no effect on overall time spent in the light-paired chamber compared to pretest values for any group during the light test or the posttest ($F(2,18) = 0.17$; $p = 0.84$; Figure 5F). Our data show for the first time a PAG_{GABA}→VTA behavioral phenotype of immobility that is blocked in the presence of opioids.

Discussion

Afferent-specific regulation of the VTA

Inhibition of VTA dopamine cells is a key regulator governing diverse behaviors. Our findings raise the question of why two GABAergic afferents to the same target brain region may have such different effects on behavior. We favor the idea that the RMTg and PAG GABAergic afferents to the VTA are embedded in distinct circuits mediating distinct behaviors. Our in vivo recordings were all made from neurons in the lateral VTA, suggesting that even this subgroup contains cells that participate in distinct circuits (Lammel et al., 2014, Engelhard et al., 2019; Breton et al., 2019); the VTA cells that receive RMTg input themselves may have projection targets distinct from those innervated by PAG inputs (Beier et al., 2015), and may furthermore be innervated by a distinct complement of afferents. The PAG also targets both dopaminergic and GABAergic VTA neurons (Balcita-Pedicino et al., 2011, Ntamati et al., 2018), while the RMTg mainly innervates dopamine cells, and the complex local circuitry will have to be considered in circuit models. As the neurons we are stimulating release GABA, these responses are not likely to involve polysynaptic circuitry, but our approach cannot rule out the possibility that $VGAT^{+}$ cells could produce distinct effects via co-release of neurotransmitters such as glutamate (Jonas et al., 1998, Fattorini et al., 2015, Granger et al., 2017) or neuropeptides (Omelchenko and Sesack, 2010) and we recently have shown that RMTg afferents can co-release glycine (Polter et al., 2018). In addition, differences in spontaneous activity and synaptic strength of RMTg vs. PAG GABAergic inputs may contribute to distinct behavioral responses.

Synapses from the RMTg to the VTA exhibit LTD after low frequency stimulation

RMTg cells fire spontaneously at relatively high rates (Jhou et al., 2009a, Hong et al., 2011, Jalabert et al., 2011, Lecca et al., 2011), and changes in synaptic strength at their VTA synapses could therefore powerfully regulate the excitability of dopamine cells. Previous work demonstrated that neither high-frequency afferent stimulation (Simmons et al., 2017) nor a nitric oxide donor (Polter et al., 2018) applied to optogenetically activated $RMTg_{GABA}$→VTA synapses elicits LTP as these stimuli do at other GABAergic VTA synapses (Nugent et al., 2007). We observed LTD that persisted in an NMDAR antagonist, that may be identical to the LTD_{GABA} previously described (Dacher and Nugent, 2011). CB1 receptor activation can also depress RMTg inputs in the VTA, although the duration of the depression beyond 20 minutes is not yet known (Lecca et al., 2012). A strong inhibitory input like that from RMTg→VTA may not require a large upward dynamic range, and this

might account for the apparent absence of available LTP mechanisms at this synapse. The strong reduction of this afferent input by DAMGO indicates that in the presence of opioid drugs RMTg→VTA IPSCs will be decreased. Local delivery of morphine into the RMTg in vivo reduces firing in some cells to rates as low as 1 Hz (Jalabert et al., 2011). We found that these synapses undergo modest LTD when activated at 1 Hz, even in the presence of an opioid agonist. In the presence of opioids, RMTg→VTA synapses may therefore be depressed further and become more persistently weakened through LTD induction.

Activating RMTg inputs to the VTA is aversive

Directly activating cell bodies in the RMTg or increasing excitatory drive to RMTg cells is aversive, and the aversive nature of this stimulation has been attributed to the inhibition of VTA dopamine cell firing (Hong et al., 2011, Stamatakis and Stuber, 2012). There are, however, other projection targets of RMTg cells that could be responsible for aversion, including the dorsal raphe, periaqueductal gray, and pedunculopontine nucleus that also have been linked to emotional behavior, although the projection to the VTA is one of the densest RMTg efferents (Lavezzi and Zahm, 2011). Conditioned place aversion that developed over several days was recently reported using an optogenetic strategy similar to ours to drive RMTg GABAergic afferents, while optogenetic inhibition of RMTg to VTA neurons produced conditioned place preference (Smith et al., 2018). In our experiments, even a single brief exposure was sufficient to produce aversion, as well as creating an aversive memory that remained 24 hours later. Taken together, our results suggest that in the presence of opioids activation of RMTg→VTA synapses and resulting aversion and aversion-related memories may be strongly inhibited. Further work is needed to define the behaviors likely to be affected, including nociception (Bourdy and Barrot, 2012, Taylor et al., 2019a)

Unique LTP of synapses from the PAG to the VTA after low frequency stimulation

After finding that LFS depressed $RMTg_{GABA}$→VTA synapses, we were surprised to find that the same protocol instead potentiated $vPAG_{GABA}$→VTA synapses. There are numerous examples of LFS inducing LTD (Bear and Malenka, 1994, Gutlerner et al., 2002), yet very few instances of LFS inducing LTP (except when paired with strong depolarization promoting NMDA receptor activation) (Bonci and Malenka, 1999, Ikeda et al., 2007, Dringenberg et al., 2014, Lante et al., 2006). LFS can potentiate excitatory synapses independently of NMDAR activation via mGluR activation in dentate gyrus (Gonzalez et al., 2014) and in hippocampal CA1 neurons (Lante et al., 2006). Recently, our lab reported that electrical LFS of IPSCs in VTA cells could elicit LTP rather than LTD when the stimulation site was caudal to the recorded cell (St. Laurent and Kauer, 2019). The present work suggests that this caudal stimulation site may preferentially activate PAG afferents. To our knowledge, ours are the first reports of LTP at GABAergic synapses elicited by LFS, and demonstrate that there are plasticity mechanisms in the VTA that are still being identified. $LFS\text{-}LTP_{GABA}$ of vPAG→VTA synapses is expected to sharply increase their importance in controlling the circuit.

Postsynaptic hyperpolarization or chelation of postsynaptic Ca^{2+} during oLFS blocked LTP. Moreover, μOR activation also prevented LTP, although inhibiting GPCR activity postsynaptically had no effect on LTP induction. We speculate that the opioid block of LTP

indicates that both postsynaptic and presynaptic mechanisms may be required for LTP. For instance, opioids may reduce presynaptic release of not only GABA, but also a peptide required in addition to postsynaptic depolarization (which may occur in vivo via burst firing). Further work is clearly required to understand the mechanism of this LTP. Opiates in vivo would be expected both to depress release of GABA from these afferents and to prevent LTP, sharply reducing the impact of $vPAG_{GABA}$→VTA afferents.

PAG_{GABA} inputs to the VTA increases immobility

Activating the GABAergic PAG→VTA input in vivo increased immobility, a phenotype associated with nonspecific direct stimulation of the ventrolateral PAG (DePaulis et al., 1994), and optogenetic stimulation of ventrolateral PAG cell bodies at 20 Hz increased freezing in rats (Assareh et al., 2017). PAG-mediated behaviors can require only descending motor-related projections, for example, freezing behavior depends on a projection to the magnocellular nucleus of the medulla (Tovote et al., 2016). However, there also are examples of behaviors regulated by ascending projections from the PAG (Rizvi et al., 1991, Vianna and Brandao, 2003) such as the PAG dopaminergic input to the central amygdala that is integral for fear learning (Groessl et al., 2018) and to the bed nucleus of the stria terminalis that is antinociceptive (Li et al., 2016).

The presence of an inhibitory circuit involving both the PAG and the VTA is intriguing because both are known sites of opioid action, but previously little was known about the behaviors specifically regulated by $vPAG_{GABA}$→VTA afferents. Our results show that the immobility can be triggered without involving excitatory or dopaminergic cells in the vPAG nor most likely, their other afferent targets. Instead of relating to freezing behavior, PAG_{GABA}→VTA afferents could contribute to pain-related circuitry (Kender et al., 2008, Li et al., 2016, Pezze and Feldon, 2004, Tan et al., 2012). A recent study in rats found that non-cell type specific vlPAG projections activated with optogenetic stimulation in the VTA produced conditioned place aversion that developed over a period of days, and linked the aversion to craniofacial pain in a migraine model (Waung et al., 2019). Consistent with this idea, chemogenetic activation of GABAergic vlPAG neurons produces hypersensitivity to mechanical and noxious thermal stimuli, while inhibiting these cells decreases sensitivity to noxious thermal stimuli (Samineni et al., 2017) (although chemogenetic changes were produced using systemic injections, so that projections to multiple brain regions were likely activated/inhibited). These observations raise the possibility that the immobility we observed on a shorter time scale may also be related to nociception.

The $vPAG_{GABA}$→VTA connection expresses an unusual form of LTP after LFS in vitro, and we began to test the behavioral impact of LFS of PAG_{GABA}→VTA synapses in vivo. Preceding the RTPP with 1 Hz light stimulation may potentiate the effect of 20 Hz light stimulation, as seen by the significant effect of test order in Figure S5F. Interestingly, increased immobility with LFS preconditioning appeared to carry over into the second test day indicating that perhaps plasticity persisted for at least 24 hours. While the immobility phenotype we report is one readout of activating vPAG→VTA afferents, further work is needed to fully appreciate the behavioral relevance of this pathway, as well as the LTP that it can express.

Potential role of VTA afferents originating in the PAG for the acute actions of opioids

Drug-induced changes in the reward pathway may precede the transition to addiction (Di Chiara and Imperato, 1988). For instance, morphine injections into the PAG result in tolerance that may contribute to increased opiate consumption (Siuciak and Advokat, 1987, Lane et al., 2004). Many drugs of abuse, including morphine, block at least one form of LTP at inhibitory synapses (Nugent et al., 2007, Guan and Ye, 2010, Niehaus et al., 2010, Dacher and Nugent, 2011). Here we show that PAG_{GABA}→VTA synapses are profoundly depressed and $LFS\text{-}LTP_{GABA}$ is prevented by acute μOR activation, although $LFS\text{-}LTD_{GABA}$ of RMTg synapses is unaffected. Future studies will be needed to determine how prior in vivo exposure to morphine affects these two forms of synaptic plasticity over a longer time period (Nugent et al., 2007; Dacher and Nugent, 2011). Moreover, increased immobility seen with PAG_{GABA}→VTA photostimulation is absent after morphine treatment in vivo. It is likely that morphine reduces GABA release to levels that are no longer effective in altering the firing of VTA cells, thus interrupting the normal role of afferent stimulation triggering immobility. Although in our experiments morphine could act at multiple sites, the reversal of immobility by morphine is consistent with the idea that opiate drugs are capable of removing the influence of the PAG_{GABA}→VTA pathway. The resulting disinhibition of dopamine neurons could in theory promote opiate reward. Our observations underline the importance of dissecting the complex circuitry of the VTA, as well as the divergent ability of distinct afferents to express synaptic plasticity and susceptibility to opiate drugs (Birdsong et al., 2019).

STAR Methods

Lead Contact and Materials Availability

Further information and requests for resources and reagents should be directed to and will be fulfilled by the Lead Contact, Julie A. Kauer, Ph.D. (jkauer@stanford.edu).

This study did not generate new unique reagents.

Experimental Model and Subject Details

Animals—All procedures were carried out in accordance with the guidelines of the National Institutes of Health for animal care and use, and were approved by the Brown University and Stanford University Institutional Animal Care and Use Committees. This study used VGAT::IRES-Cre (Jackson Laboratory, stock number: 028862, strain code: B6J.129S6(FVB)-Slc32a1$^{tm2(cre)Lowl}$), DAT::IRES-Cre (Jackson Laboratory, stock number:006660, strain code: B6.SJL-Slc6a3$^{tm1.1(cre)Bkmn/J}$), Ai14 (Jackson Laboratory, stock number: 007908, strain code: B6;129S6-Gt(ROSA)26Sor$^{tm14(CAG-tdTomato)Hze/J}$), Pitx3:GFP (Zhao et al., 2004) and C57BL/6 male and female mice bred in-house. Mice were maintained on a 12-h light/dark cycle and provided food and water ad libitum.

Method Details

RTPP—We used custom-made, two-chamber behavioral arenas (35 × 30 × 30 cm) for RTPP experiments. For all tests, we assigned one counterbalanced side of the arena as the light stimulation side and each test lasted for a total duration of 10 min. At the onset of the

test, mice were placed in the center of the arena between the two chambers and the test was immediately started. For tests where light stimulation was present, light pulses were triggered by entry into the designated light-paired chamber and delivered constantly at the appropriate frequency (60 Hz for RMTg, 20 Hz for PAG experiments) until the mouse crossed into the non-stimulation side where light delivery was immediately terminated. We recorded behavioral data and light stimulation was triggered via a CCD camera interfaced with Ethovision software (Noldus Information Technologies). Light stimulation was triggered by 10 ms TTL pulses generated by a Master-8 connected to an LED driver (Plexon LD-1). For RMTg experiments, mice underwent 3 test sessions each separated by 24 h: pretest, 60 Hz light stimulation, and posttest. For PAG drug-free experiments, mice underwent 4 test sessions each separated by 24 h: pretest, 20 Hz light stimulation, LFS preconditioning & 20 Hz light stimulation, and posttest. Days 2 and 3 were counterbalanced. For PAG morphine experiments, mice received a single intraperitoneal injection of saline in the animal facility and were returned to their home cage once per day for two days preceding testing. On day 1 (pretest), mice received an injection of saline i.p. 30 min prior to being tested in the RTPP apparatus; on day 2, mice received a single i.p. injection of morphine (3 mg/kg at 1 mg/ml) or the equivalent volume of saline 30 min prior to being tested. For all sessions (pretests, light tests, LFS preconditioning, posttests), mice were connected to a light fiber with black tubing covering the ferrule connector to reduce the amount of light visible from the head cap. We calculated immobility by averaging the velocity of the center point of the mouse every 10 samples; values less than 1.75 cm/s over this period were categorized as time spent immobile.

Rotarod—A subset of mice (RMTg: n = 6 mice/group; PAG: n = 5 mice/group) used for behavioral assays were tested on a rotarod. First, mice were placed on a 5 lane rotarod for mice (Med Associates) at a starting speed of 4 rpm. After a brief session where the mouse learned to walk forward to avoid falling off, we next trained the mice to walk at 20 rpm by gradually accelerating the speed until the mouse was able to maintain 20 rpm. After a period of rest, the mouse was attached to a fiber optic cable and returned to the rotarod. After a stable 3 min baseline period at 20 rpm to acclimate to the fiber optic cable, light stimulation was turned on for 1 min (20 or 60 Hz for PAG and RMTg mice, respectively). Light stimulation was followed by 1 min of light off. Number of falls or complete inversions on the rotarod per minute were compared between light on and light off conditions.

Immunohistochemistry—Mice were deeply anesthetized with ketamine (75 mg/kg) and dexmedetomidine (0.25mg/kg) i.p. and transcardially perfused with 50 mL of PBS followed by 50 mL of 4% PFA. Whole brains were dissected out and post-fixed overnight, then transferred to 30% sucrose in PBS for 48 hours until sunk. Brains were embedded in 3% agarose and cut to 50 μm thickness on a Vibratome ® 1000 plus Sectioning System and stored in PBS. For virus and optic fiber implant verification, slices were mounted on slides with VectaShield mounting medium (Vector Laboratories, Inc.). For immunostaining, free floating slices were washed three times (10 min) in PBS, three times (10 min) in warmed PBS containing 5% Triton-X 100 (PBS-T) and blocked in 5% normal donkey serum (NDS) and 5% bovine serum albumin (BSA) in PBS at room temperature for 1 hour. Sections were then incubated in primary antibody against FoxP1 (rabbit anti-FoxP1, 1:20,000 Abcam

ab16645) in 0.1% PBS-T at 4°C for 96 hours or overnight, respectively. Sections were washed three times (10 min) in PBS, blocked in 5% NDS in 0.25% PBS-T for three washes (10 min), then incubated in secondary antibodies (donkey anti-rabbit conjugated to Alexa-594 or Alexa-405 fluorescent dyes, 2mg/ml ThermoFisher) for 3 hours at room temperature. Slices were rinsed five times (10 min) in PBS and then mounted on slides with Fluoromount-G mounting medium (Southern Biotech). Imaging of immunofluorescence and virally expressed fluorescent proteins was performed using a Zeiss LSM 800 or Zeiss Axiolmager Apotome using the 10×, 20× and 40× (water immersion) objectives. eYFP was imaged using a 488 nm diode laser; Alexa594 and mCherry were imaged using a 561 nm diode laser; and Alexa 405 was imaged using the 405 diode laser. Images were processed and analyzed using Zeiss Zen Blue software, AxioVision software, and Adobe Illustrator CC 2017. Fox P1 staining was used as a marker of RMTg neurons (Lahti et al., 2016).

Method Details

Stereotaxic injections—Stereotaxic surgeries were performed on male and female mice between postnatal days 25–35. For RMTg injections, VGAT::IRES-Cre or VGAT::IRES-cre/Pitx::GFP mice were deeply anesthetized with ketamine and dexdormitor and 200–300 nL of AAV2-EF1a-DIO-hChR2(H134R)-EYFP or AAV2-EF1a-DIO-hChR2(H134R)-mCherry (UNC vector core) were bilaterally injected into the RMTg (AP:−2.5, ML: ±0.5 DV:−4.4). Horizontal slices containing the VTA were prepared 3–8 weeks after surgery. For PAG experiments, 200–300 nL of AAV2/9-hsyn-ChR2-EYFP was injected into C57BL6 or DAT-cre/Ai14 mice or AAV5-DIO-hChR2(H134R)-mCherry was injected unilaterally into the PAG of VGAT::IRES-Cre or VGAT::IRES-cre/Pitx::GFP mice (AP: −3.7, ML: 0.4, DV: −1.8). Horizontal slices containing the VTA were prepared 3–8 weeks after surgery. Slices from injection regions were also prepared to confirm their viral expression locations; data from mice with mistargeted injection sites of virus were discarded. RMTg electrophysiology # surgeries, 33; approximate number excluded for mistargeting, 5. PAG electrophysiology, surgeries 100, approximately 19 excluded for mistargeting.

Optic fiber implantation—For behavioral experiments, mice received a unilateral viral injection into the RMTg or PAG as described above. Reporter only groups for RMTg experiments received the 200–300 nL of AAV2-DIO-mCherry. Reporter only groups for PAG experiments received the 200–300 nL of AAV2-DIO-mCherry or AAV2-DIO-EYFP. During the same surgery, a ceramic ferrule with a 200 μM light fiber (ThorLabs) was implanted over the VTA on the same hemisphere and affixed to the skull with Metabond and dental acrylic. Light output for all ferrules was in the range of 4 – 10 mW at the tip measured using an optical power meter (ThorLabs). The exposed end of the ferrule was protected with a dust cap except when the mouse was tethered to the LED cable. All behavioral assays were performed between 4 and 9 weeks after surgery to allow for adequate viral expression. We found that RMTg viral injections have robust terminal expression starting at 4 weeks and PAG viral injections have robust terminal expression starting at 6 weeks. Behavioral data from mice where the virus or implant site was mistargeted were excluded from analysis. If injections targeted other brain areas outside of PAG or RMTg, data were not collected (slice work) or included in our analysis (behavioral work). Our injection sites were determined by light microscopy in fixed tissue for behavioral

experiments, and light microscopy of fresh tissue for electrophysiological experiments. “Illustrative images of viral injections in Figures 1 and 3 are composite images of DIC and fluorescent signal. In some experiments our injections also had some spread to the lateral or dorsal PAG rather than solely ventrolateral PAG (inputs from dorsal PAG to VTA are known to be sparse (Ntamati et al., 2018; Waung et al., 2019)). We included animals with spread into lateral and dorsal regions of the PAG, as these subregions have few to no projections to the VTA (unpublished observations from our lab; Ntamati et al., 2018), but we excluded any experiments that included dorsal raphe infection. Our results from animals with some spread into lateral/dorsal PAG did not differ from those with pure vlPAG, so we are reasonably confident that the vlPAG is the region most likely responsible for our results. Because we wanted to collect data only from RMTg and not VTA GABAergic afferents, we discarded any tissue or behavioral data for which there was any expression in the VTA. This prevented overlap with the VTA proper, and likely biased our focal injections in the caudal direction for RMTg sites. Mice excluded because of mistargeting of virus or optical fibers: RTPP: PAG, 17 mice included,13 mice excluded for mistargeting; RTTP+morphine: PAG, 21 mice included, 9 mice excluded for mistargeting; RTTP: RMTg, 12 mice included, 9 mice excluded for mistargeting. As with all in vivo optogenetic experiments, there remains the possibility of activation of fibers of passage. Because of the ventral location of the VTA (so that relatively few regions other than VTA will experience light) as well as our care in using only animals with correct VTA-only light fiber placements, we believe that we have minimized the issue to the extent possible.

Brain slice preparation—Horizontal slices (220 μm) were prepared from deeply anesthetized mice. Mice were perfused with ice-cold oxygenated artificial cerebrospinal fluid (ACSF, in mM): 126 NaCl, 21.4 $NaHCO_3$, 2.5 KCl, 1.2 NaH_2PO_4, 2.4 $CaCl_2$, 1.0 $MgSO_4$, 11.1 glucose and 5 sodium ascorbate. Following perfusion, the brain was rapidly dissected and horizontal slices (220 μm) were prepared using a vibratome. Slices recovered for 1 h at 34C in oxygenated HEPES holdi ng solution (in μM): 86 NaCI, 2.5 KCl, 1.2 NaH_2PO_4, 35 $NaHCO_3$, 20 HEPES, 25 glucose, 5 sodium ascorbate, 2 thiourea, 3 sodium pyruvate, 1 $MgSO_4.7H_2O$, 2 $CaCl_2.2H_2O$ (Ting et al., 2014), and then were held in the same HEPES solution at room temperature until use. Slices were then transferred to a recording chamber where they were submerged in ACSF without sodium ascorbate, at 30°C with a flow rate of 1–2 ml/min.

Electrophysiological recordings—Electrophysiological experiments were performed as described previously (Graziane et al., 2013; Nugent et al., 2007). Horizontal or coronal midbrain slices were continuously perfused with ACSF containing 10 μM AMPA and 1 μM glycine receptor antagonists, 6,7-dinitroquinoxaline- 2,3-dione (DNQX) and strychnine, respectively. For all plasticity experiments, GABAergic inputs were isolated using pharmacological antagonists of glycine and AMPARs (1 μM strychnine, 10 μM DNQX) and voltage-clamped at −70 mV except during oLFS. For DA neurons, −40 mV is in fact closer to their “resting” membrane potential than is −70 mV, as these neurons often fire spontaneously in vivo or in vitro. Both −70 mV and −40 mV are within the physiological range, traversed during normal action potential firing and via inhibitory synaptic potentials. In our experiments we either voltage-clamped at - 70 throughout to minimize action

potential firing during synaptic stimulation, including during the oLFS protocol, or we voltage-clamped at −70 mV except during the oLFS protocol.

Most recordings also included the NMDA receptor antagonist APV (100 μM, except where noted). Whole-cell recordings were performed with KCl pipette solution and voltage-clamped at −70 mV unless otherwise noted. Patch pipettes were filled with (in mM): 125 KCl, 2.8 NaCl, 2 $MgCl_2$, 2 ATP-Na+, 0.3 GTP-Na+, 0.6 EGTA, and 10 HEPES. In some experiments, 30 mM BAPTA or 1 mM GDP-βS were added to the pipette solution and cells were held for at least 20 minutes prior to oLFS to optimize drug delivery. In some experiments, 125 mM K gluconate was substituted for KCl to minimize alterations in E_{cl-}. For experiments using outward olPSCs, patch pipettes were filled with (in mM): 117 K-gluconate, 2.8 NaCI, 5 MgCl2, 0.2 $CaCl_2$, 2 ATP-Na+, 0.3 GTP-Na+, 0.6 EGTA, and 10 HEPES. Presence of a hyperpolarization current was used to select neurons for recording. In most experiments, we used cells that had a steady-state h-current greater than 25 pA during a step from −50 mV to −100 mV because in the lateral VTA, this measure can indicate dopamine cell classification (Ungless & Grace, 2012; Baimel et al., 2017; Edwards et. al, 2017). Note that this voltage step is different from that used by some other groups (Lammel et al., 2014), and we nearly always obtain a larger I_h value if the larger step is used (−40 to −120; with a 50 mV step protocol mean I_h of reported cells: 64 ± 10 pA; with the 80 mV step protocol, mean I_h of reported cells: 171 ± 28 pA). Furthermore, in 38 of 109 experiments, VTA dopamine cells were identified via fluorescent labeling using dopamine transporter expression in DAT::IRES-Cre/Ai14 mice or tyrosine hydroxylase expression in VGAT::IRES-cre/Pitx3-GFP mice (see Figures S1E, S3E, S4C,F,I), and our I_h values do not vary significantly from the I_h defined population. Nonetheless, this approach leaves the possibility that a subset of our recordings were from non-dopaminergic cells (Margolis et. al, 2006), and therefore we refer to them instead as VTA cells.

Channelrhodopsin-induced synaptic currents were evoked through the microscope objective using 0.1–10 ms full-field light pulses from a white LED (Mightex) controlled by driver (ThorLabs) and reflected through a 40x water immersion lens (Polter et al., 2018). Pairs or trains of light-evoked IPSCs were separated by 30s to avoid desensitization of the opsin. When feasible, oIPSCs were shown to be $GABA_a$ receptor-mediated by bath application of 30 μM bicuculline at the end of recordings. The series resistance was monitored continuously during the experiment and cells were discarded for deviations >15%.

Low frequency stimulation protocols—For LFS experiments, after a stable 10 min baseline, stimulation was delivered at 1 Hz while voltage-clamping the postsynaptic cell to −40 mV for 6 min. Experiments using LFS without postsynaptic cell depolarization maintained −70 mV voltage clamp during LFS.

Quantification and Statistical Analysis—All electrophysiology data were analyzed using CLAMPFIT software and statistical tests were computed using GRAPHPAD PRISM. Significance was determined using a Student's t-test or one-way ANOVA. Results are expressed as mean +/− S.E.M. and significance of $p < 0.05$ was considered significant and is denoted by an asterisk. LTP values are reported as averaged IPSC amplitudes for 10 min just before LTP induction compared with averaged IPSC amplitudes during the 10-min period

from 10–20 min after manipulation. Behavior was compared by one or two-way ANOVA with significant F values followed up with Sidak's or Tukey's multiple comparisons post hoc tests to compare experimental and control groups.

Data and Code Availability

Data from this study are available from the corresponding author upon request.

Supplementary Material

Refer to Web version on PubMed Central for supplementary material.

Acknowledgements

We thank Caroline Casper and Mollie Westrick for technical assistance, Dr. Kevin Bath and Dr. Christopher Moore for general discussion of behavioral tests, Dr. Susan Sesack for helpful discussion of anatomical considerations, and Dr. Elizabeth Steinberg for comments on the manuscript. This work was supported by NIDA 011289 (JAK), T32 MH20068 (RS) and NIDA F31DA045419 (RS).

References

ASSAREH N, BAGLEY EE, CARRIVE P & MCNALLY GP 2017 Brief optogenetic inhibition of rat lateral or ventrolateral periaqueductal gray augments the acquisition of Pavlovian fear conditioning. Behav Neurosci, 131, 454–459. [PubMed: 29083203]

BALCITA-PEDICINO JJ, OMELCHENKO N, BELL R & SESACK SR 2011 The inhibitory influence of the lateral habenula on midbrain dopamine cells: Ultrastructural evidence for indirect mediation via the rostromedial mesopontine tegmental nucleus. J. Comp. Neurol, 519, 1143–1164. [PubMed: 21344406]

BANDLER R & KEAY KA 1996 Columnar organization in the midbrain periaqueductal gray and the integration of emotional expression. Prog Brain Res, 107, 285–300. [PubMed: 8782526]

BANDLER R & SHIPLEY MT 1994 Columnar organization in the midbrain periaqueductal gray: modules for emotional expression? Trends Neurosci, 17, 379–89. [PubMed: 7817403]

Barbaresi P, Conti F, Manzoni T. 1982 Axonal branching in the periaqueductal gray projections to the thalamus: a fluorescent retrograde double-labeling study in the cat. Brain Res 252:137–141. [PubMed: 7172015]

BEAR MF & MALENKA RC 1994 Synaptic plasticity: LTP and LTD. Curr Opin Neurobiol, 4, 389–99. [PubMed: 7919934]

BEIER KT, STEINBERG EE, DELOACH KE, XIE S, MIYAMICHI K, SCHWARZ L, GAO XJ, KREMER EJ, MALENKA RC & LUO L 2015 Circuit Architecture of VTA Dopamine Neurons Revealed by Systematic Input-Output Mapping. Cell, 162, 622–634. [PubMed: 26232228]

Birdsong WT, Jongbloets bC, Engeln KA, Wang D, Scherrer G, Mao T. 2019 Synapse-specific opioid modulation of thalamo-cortico-striatal circuits. Elife, doi: 10.7554/eLife.45146.

BONCI A & MALENKA RC 1999 Properties and plasticity of excitatory synapses on dopaminergic and GABAergic cells in the ventral tegmental area. J. Neurosci, 19, 3723–30. [PubMed: 10234004]

Bourdy R, Barrot M. 2012 A new control center for dopaminergic systems: pulling the VTA by the tail. Trends Neurosci, 35, 681–90. [PubMed: 22824232]

Breton JM, Charbit AR, Snyder BJ, Fong PTK, Dias EV, Himmels P, Lock H, Margolis EB. 2019Relative contributions and mapping of ventral tegmental area dopamine and GABA neurons by projection target in the rat. J Comp Neurol, 527, 916–941. [PubMed: 30393861]

Kn Campion, Saville KA Morgan MM. 2016 Relative contribution of the dorsal raphe nucleus and ventrolateral periaqueductal gray to morphine antinociception and tolerance in the rat. Eur J Neurosci, 9, 2667–2672.

DACHER M, GOUTY S, DASH S, COX BM & NUGENT FS 2013 A-Kinase Anchoring Protein-Calcineurin Signaling in Long-Term Depression of GABAergic Synapses. J Neurosci, 33, 2650–2660. [PubMed: 23392692]

DACHER M & NUGENT FS 2011 Morphine-induced modulation of LTD at GABAergic synapses in the ventral tegmental area. Neuropharmacol, 61, 1166–1171.

DE OLIVEIRA AR, REIMER AE, REIS FM & BRANDAO ML 2017 Dopamine D2-like receptors modulate freezing response, but not the activation of HPA axis, during the expression of conditioned fear. Exp Brain Res, 235, 429–436. [PubMed: 27766352]

Deng H, Xiao X, Wang Z. 2016 Periaqueductal Gray Neuronal Activities Underlie Different Aspects of Defensive Behaviors. J Neurosci, 36, 7580–8. [PubMed: 27445137]

DEPAULIS A, KEAY KA & BANDLER R 1994 Quiescence and hyporeactivity evoked byactivation of cell bodies in the ventrolateral midbrain periaqueductal gray of the rat. Exp Brain Res 99, 75–83. [PubMed: 7925798]

DI CHIARA G & IMPERATO A 1988 Drugs abused by humans preferentially increase synaptic dopamine concentrations in the mesolimbic system of freely moving rats. Proc Nat Acad Sci USA 85, 5274–5278. [PubMed: 2899326]

DRINGENBERG HC, BRANFIELD DAY LR & CHOI DH 2014 Chronic fluoxetine treatment suppresses plasticity (long-term potentiation) in the mature rodent primary auditory cortex in vivo. Neural Plast, 2014, 571285. [PubMed: 24719772]

ENGELHARD B, FINKELSTEIN J, COX J, FLEMING W, JANG HJ, ORNELAS S, KOAY SA, THIBERGE SY, DAW ND, TANK DW & WITTEN IB 2019 Specialized coding of sensory, motor and cognitive variables in VTA dopamine neurons. Nature, 570, 509–513. [PubMed: 31142844]

FAGET L, OSAKADA F, DUAN J, RESSLER R, JOHNSON AB, PROUDFOOT JA, YOO JH, CALLAWAY EM & HNASKO TS 2016 Afferent Inputs to Neurotransmitter-Defined Cell Types in the Ventral Tegmental Area. Cell Reports, 15, 2796–2808. [PubMed: 27292633]

FATTORINI G, ANTONUCCI F, MENNA E, MATTEOLI M & CONTI F 2015 Co-expression of VGLUT1 and VGAT sustains glutamate and GABA co-release and is regulated by activity in cortical neurons. J Cell Sci, 128, 1669–73. [PubMed: 25749864]

FORD CP, MARK GP & WILLIAMS JT 2006 Properties and opioid inhibition of mesolimbic dopamine neurons vary according to target location. J Neurosci 26, 2788–97. [PubMed: 16525058]

GIBSON HE, EDWARDS JG, PAGE RS, VAN HOOK MJ & KAUER JA 2008 TRPV1 channels mediate long-term depression at synapses on hippocampal interneurons. Neuron, 57, 746–59. [PubMed: 18341994]

GONZALEZ J, MORALES IS, VILLARREAL DM & DERRICK BE 2014 Low-frequency stimulation induces long-term depression and slow onset long-term potentiation at perforant path-dentate gyrus synapses in vivo. J Neurophysiol, 111, 1259–73. [PubMed: 24335215]

GRANGER AJ, WALLACE ML & SABATINI BL 2017 Multi-transmitter neurons in the mammalian central nervous system. Curr Opin Neurobiol, 45, 85–91. [PubMed: 28500992]

GROESSL F, MUNSCH T, MEIS S, GRIESSNER J, KACZANOWSKA J, PLIOTA P, KARGL D, BADUREK S, KRAITSY K, RASSOULPOUR A, ZUBER J, LESSMANN V & HAUBENSAK W 2018 Dorsal tegmental dopamine neurons gate associative learning of fear. Nat Neurosci, 21, 952–962. [PubMed: 29950668]

GUAN Y-Z & YE J-H 2010 Ethanol blocks long-term potentiation of GABAergic synapses in the ventral tegmental area involving mu-opioid receptors. Neuropsychopharmacol 35, 1841–1849.

GUTLERNER JL, PENICK EC, SNYDER EM & KAUER JA 2002 Novel protein kinase A-dependent long-term depression of excitatory synapses. Neuron, 36, 921–31. [PubMed: 12467595]

GYSLING K & WANG RY 1983 Morphine-induced activation of A10 dopamine neurons in the rat. Brain Res, 277, 119–27. [PubMed: 6315137]

HEIFETS BD & CASTILLO PE 2009 Endocannabinoid signaling and long-term synaptic plasticity. Annu Rev Physiol, 71, 283–306. [PubMed: 19575681]

HONG S, JHOU TC, SMITH M, SALEEM KS & HIKOSAKA O 2011 Negative reward signals from the lateral habenula to dopamine neurons are mediated by rostromedial tegmental nucleus in primates. J Neurosci 31, 11457–71. [PubMed: 21832176]

Huang J, Gadotti VM, Chen L, Souza IA, Huang S, Wang D, Ramakrishnan C, Deisseroth K, Zhang Z, Zamponi GW. 2019 A neuronal circuit for activating descending modulation of neuropathic pain. Nat Neurosci, 22,1659–68. [PubMed: 31501573]

IKEDA R, TAKAHASHI Y, INOUE K & KATO F 2007 NMDA receptor-independent synaptic plasticity in the central amygdala in the rat model of neuropathic pain. Pain, 127, 161–72. [PubMed: 17055162]

JALABERT M, BOURDY R, COURTIN J, VEINANTE P, MANZONI OJ, BARROT M & GEORGES F 2011 Neuronal circuits underlying acute morphine action on dopamine neurons. Proc. Natl. Acad. Sci. U. S. A, 108, 16446–16450. [PubMed: 21930931]

JENNINGS JH, SPARTA DR, STAMATAKIS AM, UNG RL, PLEIL KE, KASH TL & STUBER GD 2013 Distinct extended amygdala circuits for divergent motivational states. Nature, 496, 224–228. [PubMed: 23515155]

JENSEN TS & YAKSH TL 1989 Comparison of the antinociceptive effect of morphine and glutamate at coincidental sites in the periaqueductal gray and medial medulla in rats. Brain Res, 476, 1–9. [PubMed: 2563331]

JHOU TC, FIELDS HL, BAXTER MG, SAPER CB & HOLLAND PC 2009a The Rostromedial Tegmental Nucleus (RMTg), a GABAergic Afferent to Midbrain Dopamine Neurons, Encodes Aversive Stimuli and Inhibits Motor Responses. Neuron, 61, 786–800. [PubMed: 19285474]

JHOU TC, GEISLER S, MARINELLI M, DEGARMO BA & ZAHM DS 2009b The mesopontine rostromedial tegmental nucleus: A structure targeted by the lateral habenula that projects to the ventral tegmental area of Tsai and substantia nigra compacta. J Comp Neurol, 513, 566–596. [PubMed: 19235216]

JOHNSON SW & NORTH RA 1992 Opioids excite dopamine neurons by hyperpolarization of local interneurons. J Neurosci, 12, 483–488. [PubMed: 1346804]

JONAS P, BISCHOFBERGER J & SANDKUHLER J 1998 Corelease of two fast neurotransmitters at a central synapse. Science, 281, 419–24. [PubMed: 9665886]

JONES S & BONCI A 2005 Synaptic plasticity and drug addiction. Curr Opin Pharmacol, 5, 20–5. [PubMed: 15661621]

KEAY KA & BANDLER R 2001 Parallel circuits mediating distinct emotional coping reactions to different types of stress. Neurosci Biobehav Rev, 25, 669–678. [PubMed: 11801292]

KENDER RG, HARTE SE, MUNN EM & BORSZCZ GS 2008 Affective analgesia following muscarinic activation of the ventral tegmental area in rats. J Pain, 9, 597–605. [PubMed: 18387853]

LAMMEL S, ION DI, ROEPER J & MALENKA RC 2011 Projection-Specific Modulation of Dopamine Neuron Synapses by Aversive and Rewarding Stimuli. Neuron, 70, 855–862. [PubMed: 21658580]

LAMMEL S, LIM BK & MALENKA RC 2014 Reward and aversion in a heterogeneous midbrain dopamine system. Neuropharmacol 76, Pt B: 351–59.

LANE DA, TORTORICI V & MORGAN MM 2004 Behavioral and electrophysiological evidence for tolerance to continuous morphine administration into the ventrolateral periaqueductal gray. Neurosci 125, 63–69.

LANTE F, CAVALIER M, COHEN-SOLAL C, GUIRAMAND J & VIGNES M 2006 Developmental switch from LTD to LTP in low frequency-induced plasticity. Hippocampus, 16, 981–9. [PubMed: 17016817]

LASCHKA E & HERZ A 1977 Sites of action of morphine involved in the development of physical dependence in rats. III. Autoradiographic studies. Psychopharmacol (Berl), 53, 33–7.

LAVEZZI HN & ZAHM DS 2011 The mesopontine rostromedial tegmental nucleus: an integrative modulator of the reward system. Basal Ganglia, 1, 191–200. [PubMed: 22163100]

LECCA S, MELIS M, LUCHICCHI A, ENNAS MG, CASTELLI MP, MUNTONI AL & PISTIS M 2011 Effects of drugs of abuse on putative rostromedial tegmental neurons, inhibitory afferents to midbrain dopamine cells. Neuropsychopharmacol 36, 589–602.

LECCA S, MELIS M, LUCHICCHI A, MUNTONI AL & PISTIS M 2012 Inhibitory Inputs from Rostromedial Tegmental Neurons Regulate Spontaneous Activity of Midbrain Dopamine Cells and Their Responses to Drugs of Abuse. Neuropsychopharmacol 37, 1164–1176.

Lefler Y, Campagner D, Branco T. 2019 The role of the periaqueductal gray in escape behavior. Curr Opin Neurobiol, 60,115–121. [PubMed: 31864105]

LEWIS VA & GEBHART GF 1977 Evaluation of the periaqueductal central gray (PAG) as a morphine-specific locus of action and examination of morphine-induced and stimulation-produced analgesia at coincident PAG loci. Brain Res, 124, 283–303. [PubMed: 191150]

LI AL, SIBI JE, YANG X, CHIAO JC & PENG YB 2016 Stimulation of the ventral tegmental area increased nociceptive thresholds and decreased spinal dorsal horn neuronal activity in rat. Exp Brain Res, 234, 1505–14. [PubMed: 26821313]

Li C, Sugam JA, Lowery-Gionta EG, McElligott ZA, McCall NM, Lopez AJ, McKlveen JM, Pleil KE, Kash TL. 2016 Mu Opioid Receptor Modulation of Dopamine Neurons in the Periaqueductal Gray/Dorsal Raphe: A Role in Regulation of Pain. Neuropsychopharmacol, 41,2122–32.

Li Y, Rao Z, Shi J. 1990 Collateral projections from the midbrain periaqueductal gray to the nucleus raphe magnus and nucleus accumbens in the rat. A fluorescent retrograde double-labelling study. Neurosci Lett 117:285–288. [PubMed: 1710039]

LOWERY-GIONTA EG, DIBERTO J, MAZZONE CM & KASH TL 2018 GABA neurons of the ventral periaqueductal gray area modulate behaviors associated with anxiety and conditioned fear. Brain Struct Funct 223: 3787–99. [PubMed: 30076467]

LUSCHER C & HUBER KM 2010 Group 1 mGluR-dependent synaptic long-term depression: mechanisms and implications for circuitry and disease. Neuron, 65, 445–59. [PubMed: 20188650]

MATSUI A, JARVIE BC, ROBINSON BG, HENTGES ST & WILLIAMS JT 2014 Separate GABA afferents to dopamine neurons mediate acute action of opioids, development of tolerance, and expression of withdrawal. Neuron, 82, 1346–1356. [PubMed: 24857021]

MATSUI A & WILLIAMS JT 2011 Opioid-Sensitive GABA Inputs from Rostromedial Tegmental Nucleus Synapse onto Midbrain Dopamine Neurons. J Neurosci 31, 17729–17735. [PubMed: 22131433]

Maxwell SL, Ho HY, Kuehner E, Zhao S, Li M. 2005 Pitx3 regulates tyrosine hydroxylase expression in the substantia nigra and identifies a subgroup of mesencephalic dopaminergic progenitor neurons during mouse development. Dev Biol. 282,467–79. [PubMed: 15950611]

MAYER DJ, WOLFLE TL, AKIL H, CARDER B & LIEBESKIND JC 1971 Analgesia from electrical stimulation in the brainstem of the rat. Science, 174, 1351–4. [PubMed: 5167502]

MAZEI-ROBISON MS & NESTLER EJ 2012 Opiate-induced molecular and cellular plasticity of ventral tegmental area and locus coeruleus catecholamine neurons. Cold Spring Harb Perspect Med, 2, a012070. [PubMed: 22762025]

MORGAN MM & CARRIVE P 2001 Activation of the ventrolateral periaqueductal gray reduces locomotion but not mean arterial pressure in awake, freely moving rats. Neurosci 102, 905–10.

NESTLER EJ 2004 Historical review: Molecular and cellular mechanisms of opiate and cocaine addiction. Trends Pharmacol Sci, 25, 210–8. [PubMed: 15063085]

NIEHAUS JL, MURALI M & KAUER JA 2010 Drugs of abuse and stress impair LTP at inhibitory synapses in the ventral tegmental area. Eur J Neurosci, 32, 108–117. [PubMed: 20608969]

NTAMATI NR, CREED M, ACHARGUI R & LUSCHER C 2018 Periaqueductal efferents to dopamine and GABA neurons of the VTA. PLoS One, 13, e0190297. [PubMed: 29304042]

NUGENT FS, PENICK EC & KAUER JA 2007 Opioids block long-term potentiation of inhibitory synapses. Nature, 446, 1086–1090. [PubMed: 17460674]

OLMSTEAD MC & FRANKLIN KB 1997 The development of a conditioned place preference to morphine: effects of microinjections into various CNS sites. Behav Neurosci, 111, 1324–1334. [PubMed: 9438801]

OMELCHENKO N & SESACK SR 2010 Periaqueductal gray afferents synapse onto dopamine and GABA neurons in the rat ventral tegmental area. J Neurosci Res, 88, 981–91. [PubMed: 19885830]

PATHAN H & WILLIAMS J 2012 Basic opioid pharmacology: an update. Br J Pain, 6, 11–6. [PubMed: 26516461]

PEZZE MA & FELDON J 2004 Mesolimbic dopaminergic pathways in fear conditioning. Prog Neurobiol, 74, 301–20. [PubMed: 15582224]

POLTER AM, BARCOMB K, TSUDA AC & KAUER JA 2018 Synaptic function and plasticity in identified inhibitory inputs onto VTA dopamine neurons. Eur J Neurosci, 47, 1208–1218. [PubMed: 29480954]

Reichling DB, Basbaum Ai. 1991 Collateralization of periaqueductal gray neurons to forebrain or diencephalon and to the medullary nucleus raphe magnus in the rat. Neurosci, 42, 183–200.

RIZVI TA, ENNIS M, BEHBEHANI MM & SHIPLEY MT 1991 Connections between the central nucleus of the amygdala and the midbrain periaqueductal gray: Topography and reciprocity. J Comp Neurol 303, 121–131. [PubMed: 1706363]

SAAL D, DONG Y, BONCI A & MALENKA RC 2003 Drugs of abuse and stress trigger a common synaptic adaptation in dopamine neurons. Neuron, 37, 577–582. [PubMed: 12597856]

SAMINENI VK, GRAJALES-REYES JG, COPITS BA, O'BRIEN DE, TRIGG SL, GOMEZ AM, BRUCHAS MR & GEREAU RW 2017 Divergent Modulation of Nociception by Glutamatergic and GABAergic Neuronal Subpopulations in the Periaqueductal Gray. eNeuro, 4, ENEURO.0129–16.2017.

Saunders BT, Richard JM, Margolis EB, Janak PH. 2018 Dopamine neurons create Pavlovian conditioned stimuli with circuit-defined motivational properties. Nat Neurosci, 21,1072–1083. [PubMed: 30038277]

SIMMONS DV, PETKO AK & PALADINI CA 2017 Differential expression of long-term potentiation among identified inhibitory inputs to dopamine neurons. J Neurophysiol, 118, 1998–2008. [PubMed: 28701538]

SIUCIAK JA & ADVOKAT C 1987 Tolerance to morphine microinjections in the periaqueductal gray (PAG) induces tolerance to systemic, but not intrathecal morphine. Brain Res 424, 311–19. [PubMed: 3676830]

Smith RJ, Vento PJ, Chao YS, Good CH, Jhou TC. 2018 Gene expression and neurochemical characterization of the rostromedial tegmental nucleus (RMTg) in rats and mice. Brain Struct Funct. 224, 219–238. [PubMed: 30302539]

LAURENT R ST. AND KAUER JA. 2019 Synaptic Plasticity at Inhibitory Synapses in the Ventral Tegmental Area Depends upon Stimulation Site. eNeuro, doi: 10.1523/ENEURO.0137-19.2019.

STAMATAKIS AM & StUbER GD 2012 Activation of lateral habenula inputs to the ventral midbrain promotes behavioral avoidance. Nat Neurosci 15, 1105–7. [PubMed: 22729176]

STEFFENSEN SC, STOBBS SH, COLAGO EEO, LEE RS, KOOB GF, GALLEGOS RA & HENRIKSEN SJ 2006 Contingent and non-contingent effects of heroin on mu-opioid receptor-containing ventral tegmental area GABA neurons. Exp Neurol 202, 139–151. [PubMed: 16814775]

SUCKOW SK, DEICHSEL EL, INGRAM SL, MORGAN MM & AICHER SA 2013 Columnar distribution of catecholaminergic neurons in the ventrolateral periaqueductal gray and their relationship to efferent pathways. Synapse, 67, 94–108. [PubMed: 23152302]

TAN KR, YVON C, TURIAULT M, MIRZABEKOV JJ, DOEHNER J, LABOUEBE G, DEISSEROTH K, TYE KM & LUSCHER C 2012 GABA neurons of the VTA drive conditioned place aversion. Neuron, 73, 1173–83. [PubMed: 22445344]

Taylor NE, Long H, Pei J, Kukutla P, Phero A, Hadaegh F, Abdelnabi A, Solt K, Brenner GJ. 2019 The rostromedial tegmental nucleus: a key modulator of pain and opioid analgesia. Pain, 160, 2524–2534 [PubMed: 31246732]

Taylor NE, Pei J, Zhang J, Vlasov KY, Davis T, Taylor E, Weng FJ, Van Dort CJ, Solt K, Brown EN. 2019The Role of Glutamatergic and Dopaminergic Neurons in the Periaqueductal Gray/Dorsal Raphe: Separating Analgesia and Anxiety. eNeuro, 6 pii: ENEURO.0018–18.2019. doi: 10.1523/ENEURO.0018-18.2019

TOVOTE P, ESPOSITO MS, BOTTA P, CHAUDUN F, FADOK JP, MARKOVIC M, WOLFF SB, RAMAKRISHNAN C, FENNO L, DEISSEROTH K, HERRY C, ARBER S & LUTHI A 2016 Midbrain circuits for defensive behaviour. Nature, 534, 206–12. [PubMed: 27279213]

Vander Weele CM, Siciliano CA, Matthews GA, Namburi P, Izadmehr EM, Espinel IC, Nieh EH, Schut EHS, Padilla-Coreano N, Burgos-Robles A, Chang CJ, Kimchi EY, Beyeler A, Wichmann R, Wildes CP, Tye KM. 2018 Dopamine enhances signal-to-noise ratio in cortical-brainstem encoding of aversive stimuli. Nature, 563,397–401 [PubMed: 30405240]

VAN ZESSEN R, PHILLIPS JL, BUDYGIN EA & STUBER GD 2012 Activation of VTA GABA Neurons Disrupts Reward Consumption. Neuron, 73, 1184–1194. [PubMed: 22445345]

VAUGHAN CW, BAGLEY EE, DREW GM, SCHULLER A, PINTAR JE, HACK SP & CHRISTIE MJ 2003 Cellular actions of opioids on periaqueductal grey neurons from C57B16/J mice and mutant mice lacking mOr-1. Br J Pharmacol, 139, 362–7. [PubMed: 12770941]

VIANNA DM & BRANDAO ML 2003 Anatomical connections of the periaqueductal gray: specific neural substrates for different kinds of fear. Braz J Med Biol Res, 36, 557–66. [PubMed: 12715074]

Waung MW, Margolis EB, Charbit AR, Fields HL. 2019 A Midbrain Circuit that Mediates Headache Aversiveness in Rats. Cell Rep, 28, 2739–47. [PubMed: 31509737]

Wright KM, McDannald MA. 2019 Ventrolateral periaqueductal gray neurons prioritize threat probability over fear output. Elife, doi: 10.7554/eLife.45013.

YAKSH TL, YEUNG JC & RUDY TA 1976 Systematic examination in the rat of brain sites sensitive to the direct application of morphine: observation of differential effects within the periaqueductal gray. Brain Res, 114, 83–103. [PubMed: 963546]

Highlights

- RMTg inhibitory synapses in the VTA undergo LTD with low frequency stimulation
- PAG inhibitory synapses in the VTA undergo LTP with low frequency stimulation
- Opioids prevent LTP at PAG to VTA inhibitory synapses
- Opioids block immobility produced by PAG→VTA inhibitory terminal activation in vivo

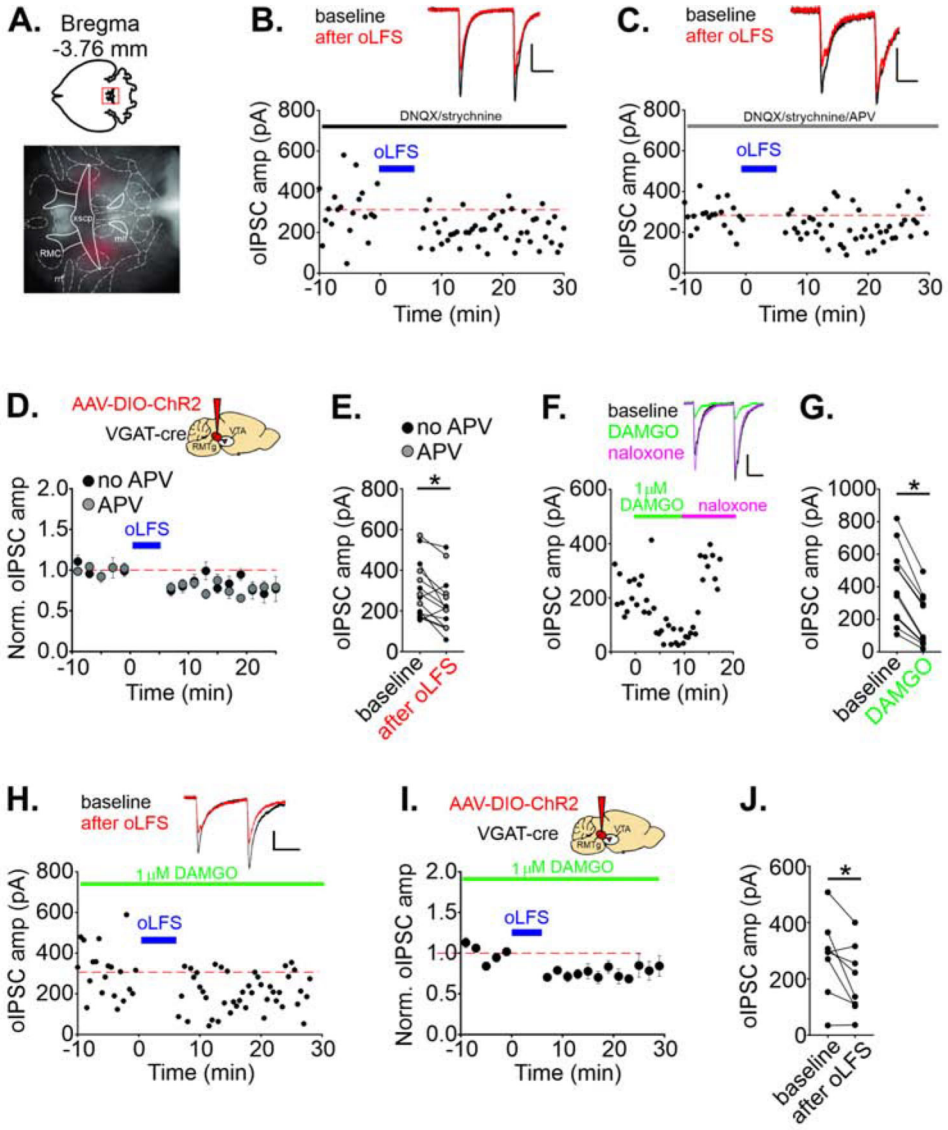

FIGURE 1. RMTg$_{GABA}$→VTA synapses exhibit LTD even in DAMGO

A. Representative viral injection in the RMTg, horizontal section. See Figure S1A for all localizations. **B.** Representative experiment, LTD of olPSCs in a cell is induced by oLFS of RMTg GABAergic afferents. Blue bars indicate time of oLFS. In this and all other electrophysiological experiments,DNQX/strychnine were included in the bath solution except as noted. **C.** Representative similar experiment in the presence of the NMDAR antagonist, d-APV. Insets: olPSCs during baseline (black) and 10–20 min after oLFS (red). **D.** Time course of LTD; averaged olPSC amplitudes before and after oLFS (n = 13 cells). **E.** Mean olPSC amplitudes for each cell comparing a 10 min baseline period and a period from 10–20 min after oLFS ($p = 0.018$, paired t-test). In all subsequent figures, d-APV was included in the bath solution. **F.** Representative experiment, 1 μM DAMGO bath application depresses olPSCs; 2 μM naloxone reverses this. **G.** Mean olPSC amplitudes before and in DAMGO ($p < 0.0001$, paired t-test) (n = 11 cells). **H.** Representative experiment, oLFS induces LTD in 1 μM DAMGO. **I.** Time course of averaged olPSC amplitudes for each cell

before and after oLFS in 1 μM DAMGO (n = 8 cells/mice), and **J.** mean olPSC amplitudes during a 10 min baseline and 10–20 min after oLFS in DAMGO ($p = 0.03$, paired t-test). Data are represented as mean ± SEM. Calibrations: 100 pA, 20 ms. *$p < .05$, paired t-test of amplitude of 10 min baseline vs.10–20 min after oLFS. See also related Supplemental Figure 1.

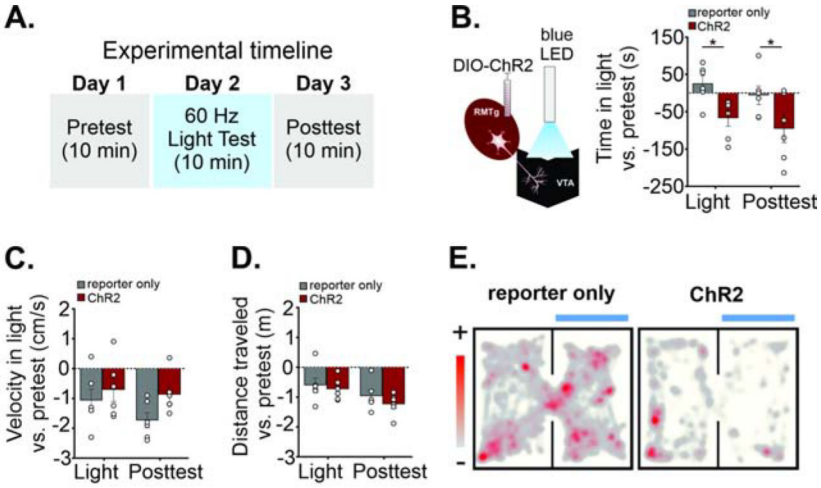

FIGURE 2. In vivo stimulation of RMTg$_{GABA}$→VTA synapses is aversive.

A. Real-time place preference (RTPP) experimental timeline. Days 1 and 3 have no light stimulation on either chamber side. On Day 2, entry into the light-paired side triggers 60 Hz blue light stimulation (light test). On day 3, mice are returned to the testing chamber without any light delivery (posttest). **B.** Left, Diagram: LED stimulation of RMTg terminals in the VTA. Right, ChR2 mice spend less time in the light-paired chamber vs. pre-test values compared to mice expressing the reporter only (light; n = 6 mice per group). 24 hours later, without any optical stimulation, mice still avoid the previously light-paired chamber (posttest). **C.** Velocity (compared to pre-test values) in the light-paired chamber, and **D.** total distance traveled in the apparatus (compared to pre-test values) are not different between experimental and reporter-only groups (2-way ANOVAs). **E.** Representative location plot of a control mCherry- expressing mouse (left) and ChR2-expressing mouse (right) during a 10 minute RTPP test session.<p/>LED light was delivered whenever the mouse entered the light-paired chamber. Data are represented as mean ± SEM. See related Supplemental Figure 2. *p < .05, 2-way ANOVA, post hoc Sidak's multiple comparisons of reporter-only vs. ChR2 mice.

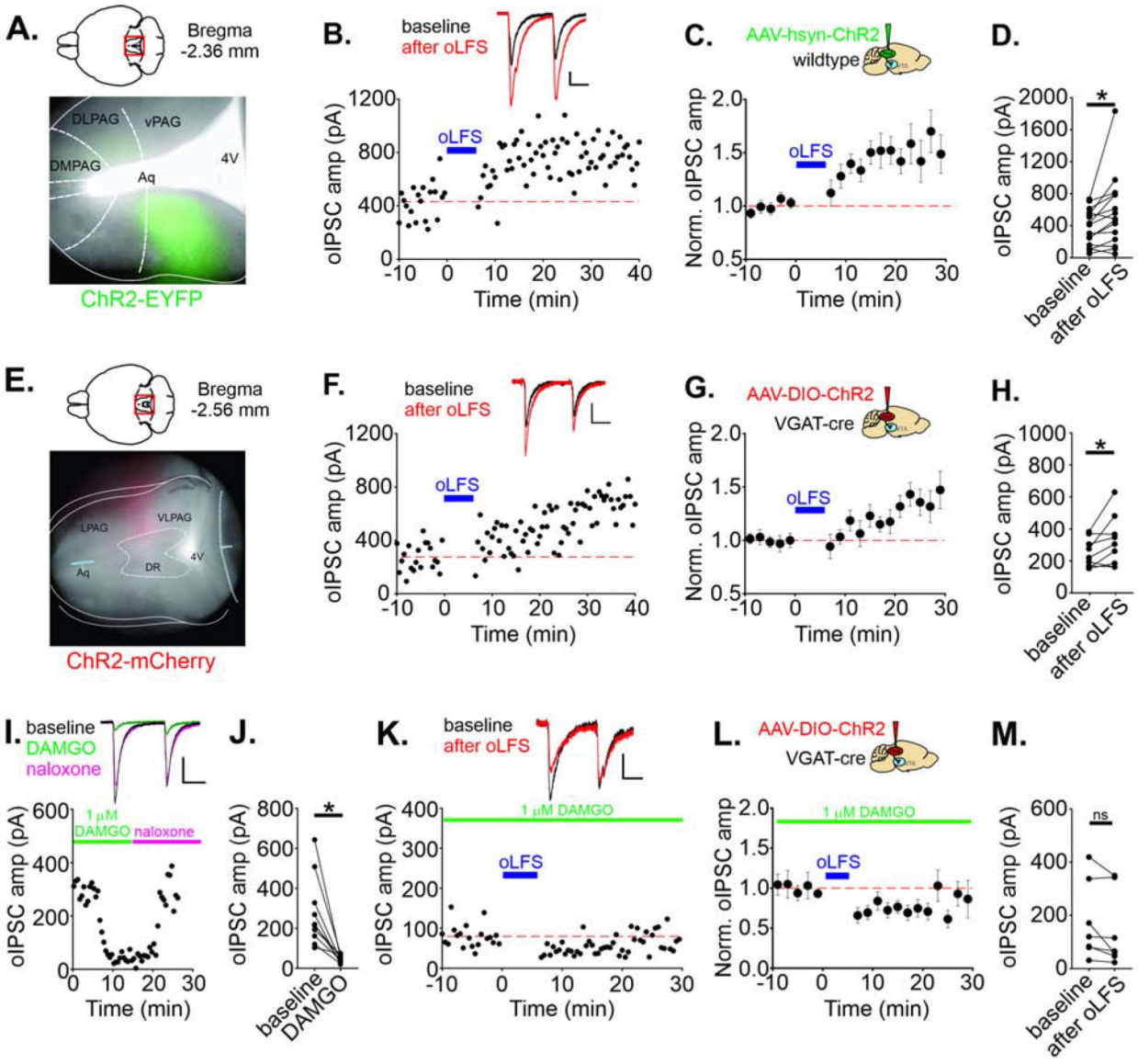

FIGURE 3. LFS induces opioid-sensitive LTP at PAG_{GABA}→VTA synapses.

A. Representative ChR2-EYFP viral expression in a wild type mouse (horizontal section). See Figure S3A for all injection localizations. **B.** Representative experiment, LTP of olPSCs in a cell is induced by oLFS (blue bar) of PAG afferents activated in slices from an AAV-hsyn-ChR2 mouse; in this and all experiments, DNQX/d-APV/strychnine are present throughout. Insets: olPSCs during baseline (black) and 10–20 min after oLFS (red). **C.** Time course of LTP; averaged olPSC amplitudes before and after oLFS (n = 15 cells). **D.** Mean olPSC amplitudes for each cell recorded during a 10 min baseline period and 10–20 min after oLFS (p = 0.023, paired t-test). **E.** Representative ChR2-mCherry viral expression in a VGAT-cre mouse allowing expression of ChR2 selectively in GABAergic PAG cells. **F.** Representative experiment, LTP of olPSCs recorded in a VTA cell using oLFS of PAG GABAergic afferents (AAV-DlO-ChR2-injected mouse). **G.** Time course of LTP; averaged olPSC amplitudes before and after oLFS (n = 9 cells) and **H.** mean olPSC amplitudes during

a 10 min baseline and 10–20 min after oLFS (p = 0.0495). **I.** Representative experiment, 1 μM DAMGO bath application followed by application of 2 μM naloxone. **J.** Mean olPSC amplitudes before and in DAMGO (p = 0.0023, paired t-test) (n = 10 cells). **K.** Representative experiment, oLFS-induced LTP is blocked in 1 μM DAMGO. **L.** Time course of averaged olPSC amplitudes before and after oLFS in 1 μM DAMGO (n = 7 cells), and **M.** mean olPSC amplitudes during a 10 min baseline and 10–20 min after oLFS in DAMGO (p = 0.0794, paired t-test). Blue bar indicates time of oLFS. Calibration: 100 pA, 20 ms except for K: 25 pA, 20 ms. Data are represented as mean ± SEM. See related Supplemental Figures 3 and 4. *p < .05, paired t-test of oIPSC amplitude of 10 min baseline vs.10–20 min after oLFS.

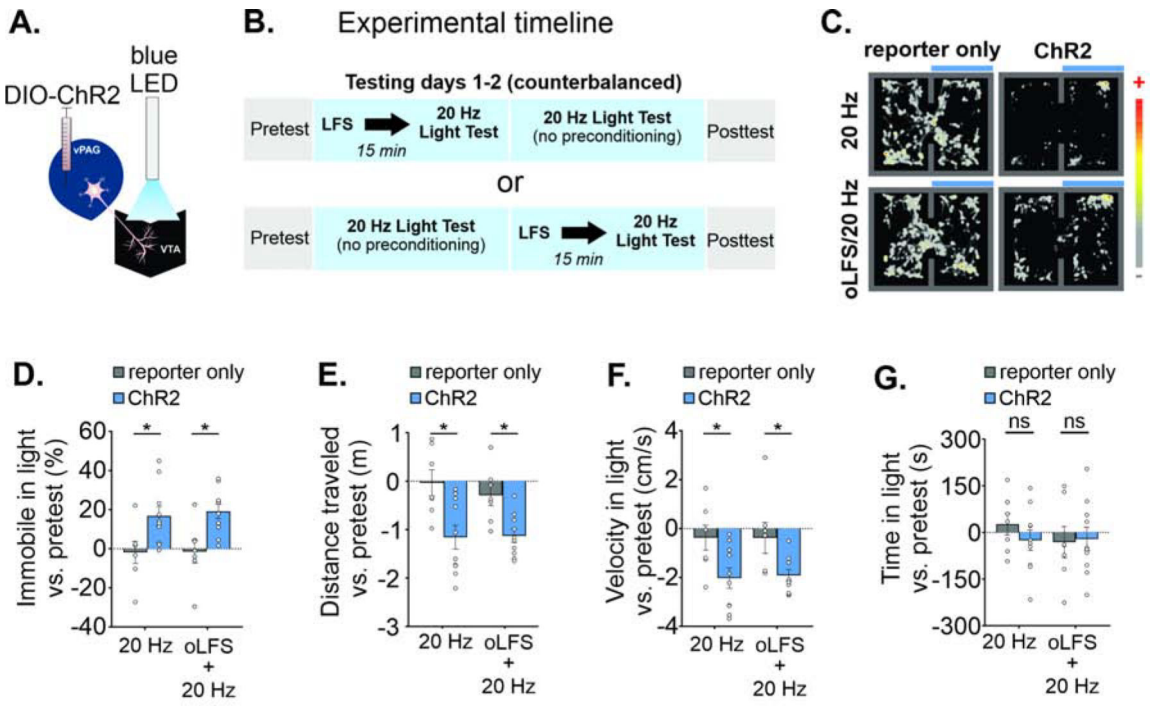

FIGURE 4. In vivo stimulation of vPAG$_{GABA}$→VTA synapses increases immobility.

A. Diagram: LED stimulation of vPAG$_{GABA}$ terminals in the VTA. **B.** Experimental timeline and design of real-time place preference (RTPP) **C.** Representative location plot of a reporter only mouse (left) and ChR2-expressing mouse (right) during a 10 minute RTPP test session with (bottom panels) or without (top panels) LFS preconditioning. LED light was delivered constantly at 20 Hz whenever the mouse entered the light-paired chamber. **D.** Time spent immobile increased compared to pretest values in ChR2 mice in the light-paired chamber (n = 7 reporter only, n = 10 ChR2 mice; Sidak's multiple comparisons 20 Hz test: p = 0.026, LFS/20 Hz test: p = 0.013). **E.** ChR2-expressing mice decrease the distance traveled in the apparatus (Sidak's multiple comparisons, 20 Hz test: p = 0.002, LFS/20 Hz test: p = 0.023), and **F.** exhibit reduced velocity in the light-paired chamber vs. pretest values (Sidak's multiple comparisons, 20 Hz test: p = 0.026, LFS/20 Hz test: p = 0.04). **G.** Average time spent in light-paired chamber vs. pretest was unchanged. Data are represented as mean ± SEM. See related Supplemental Figure 5. *p < 0.05, One- or two-way ANOVA and post hoc Sidak's multiple comparisons.

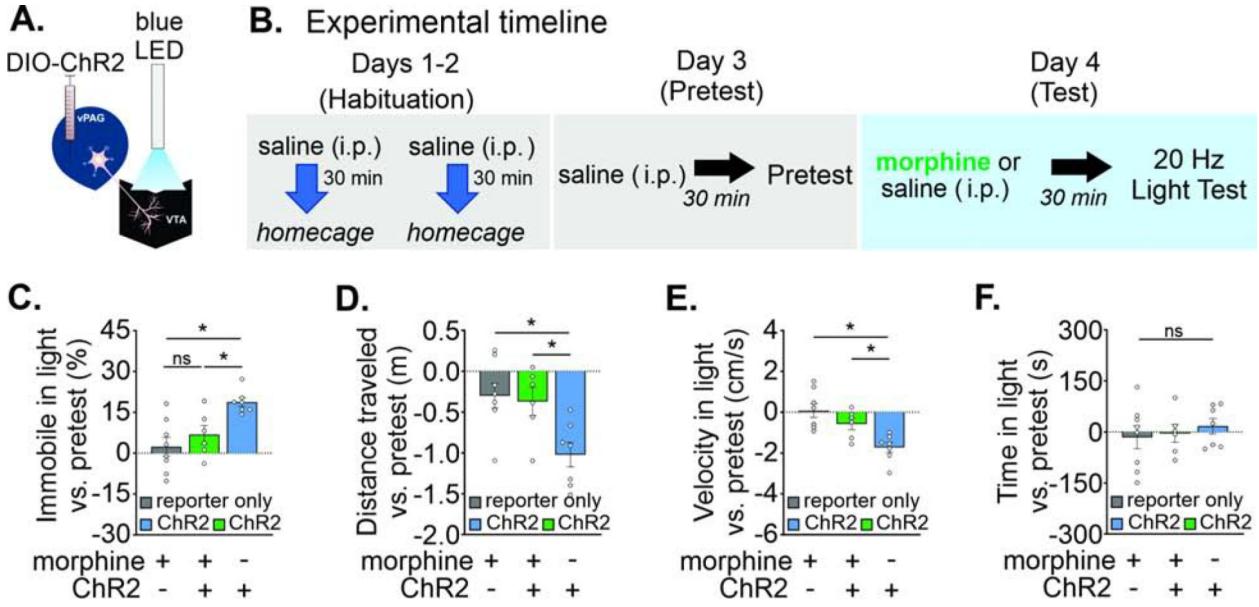

FIGURE 5. Morphine blocks vPAG$_{GABA}$→VTA stimulation-induced immobility.

A. Diagram: LED stimulation of PAG$_{GABA}$ terminals in the VTA. **B.** Experimental timeline of real time place preference procedure with morphine or saline pre-treatment. **C.** Time spent immobile increased in ChR2 mice receiving saline, but morphine blocked this (n = 8 reporter only, n = 6 morphine + ChR2, n = 7 saline + ChR2 mice, Dunnett's multiple comparisons, reporter only + MOR vs. opsin + MOR: p = 0.56, reporter only + MOR vs. opsin + SAL: p = 0.002). **D.** A corresponding decrease in distance traveled in the apparatus was observed only in ChR2 mice receiving saline (Dunnett's multiple comparisons, reporter only + MOR vs. opsin + MOR: p = 0.95, reporter only + MOR vs. opsin + SAL: p = 0.009, opsin + MOR vs. opsin + SAL: p = 0.029). **E.** A corresponding reduced velocity in the light-paired chamber was also observed only in ChR2 mice receiving saline (Dunnett's multiple comparisons, reporter only + MOR vs. opsin + MOR: p = 0.31, reporter only + MOR vs. opsin + SAL: p = 0.001, opsin + MOR vs. opsin + SAL: p = 0.044). **F.** Average time spent in the light-paired chamber vs. pretest was unaffected by light stimulation. Data are represented as mean ± SEM. See related Supplemental Figure 5. *p < 0.05, Two-way ANOVA and post hoc Dunnett's multiple comparisons.

KEY RESOURCES TABLE

REAGENT or RESOURCE	SOURCE	IDENTIFIER
Antibodies		
rabbit anti-FoxP1	Abcam	ab16645
donkey anti-rabbit conjugated to Alexa-594	Thermofisher	R-37119
donkey anti-rabbit conjugated to Alexa-405	Thermofisher	A-31556
Bacterial and Virus Strains		
AAV2-EF1a-DIO-hChR2(H134R)-EYFP	UNC Viral Vector Core	n/a
AAV2-EF1a-DIO-hChR2(H134R)-mCherry	UNC Viral Vector Core	n/a
AAV2-EF1a-DIO-mCherry	UNC Viral Vector Core	n/a
AAV2/9-hsyn-ChR2-EYFP	Penn Vector Core	AV-9-26973P
AAV5-DIO-hChR2(H134R)-mCherry	UNC Viral Vector Core	n/a
AAV-DJ-DIO-EYFP	Stanford Gene Vector and Virus Core	GVVC-AAV-013
AAV-DJ-DIO-mCherry	Stanford Gene Vector and Virus Core	GVVC-AAV-014
Chemicals, Peptides, and Recombinant Proteins		
6β-naltrexol	Sigma-Aldrich	N9412
6,7-Dinitroquinoxaline-2,3[1H,4H]-dione (DNQX)	Sigma-Aldrich	D0540
Morphine	Sigma-Aldrich	M8777
bicuculline	Tocris	0130
[D-Ala^2, NMe-Phe^4, Gly-ol^5]-enkephalin (DAMGO)	Tocris	1171
D-(-)-2-Amino-5-phosphonopentanoic acid (APV)	Tocris	0106
forskolin	R&D Systems	1099
naloxone	R&D Systems	0599
Strychnine	Abcam	ab120416
tetrodotoxin	Tocris	1078
Deposited Data		
Raw and analyzed data	This paper	
Experimental Models: Organisms/Strains		
Mouse: VGAT::IRES-Cre strain code: B6J.129S6(FVB)-Slc32a1$^{tm2(cre)Lowl}$	Jackson Laboratory	stock number: 028862
Mouse: DAT::IRES-Cre strain code: B6.SJL-Slc6a3$^{tm1.1(cre)Bkmn/J}$	Jackson Laboratory	stock number:006660
Mouse: Ai14-Cre reporter strain code: B6;129S6-Gt(ROSA)26Sor$^{tm14(CAG-tdTomato)Hze/J}$	Jackson Laboratory	stock number: 007908
Mouse: wild type C57BL/6	Jackson Laboratory	stock number: 00664
Mouse: Pitx3-GFP Strain code: B6.129P2-Pitx3$^{tm1Mli/Mmjax}$	Meng Li, Maxwell et al., 2005	MMRRC Stock No:41479-JAX
Oligonucleotides		
Recombinant DNA		

REAGENT or RESOURCE	SOURCE	IDENTIFIER
Software and Algorithms		
Ethovision XT software	Noldus Information Technologies	https://www.noldus.com/animal-behavior-research/products/ethovision-xt
pClamp 10	Molecular Devices	https://www.moleculardevices.com
ClampFit 10	Molecular Devices	https://www.moleculardevices.com
dAndor Solis	Oxford Instruments	https://andor.oxinst.com/products/solis-software/solis-i
NIS-Elements	Nikon Instruments Inc.	https://www.nikoninstruments.com/Products/Software
GraphPad Prism 7	GraphPad software	https://www.graphpad.com
Excel	Microsoft	https://products.office.com
CorelDRAW 5	CorelDRAW	https://www.coreldraw.com
Other		